

© Ocean Engineering 2024.

This manuscript version is made available under the CC-BY-NC-ND 4.0 license <https://creativecommons.org/licenses/by-nc-nd/4.0/>.

# Model predictive control-based trajectory generation for agile landing of unmanned aerial vehicle on a moving boat<sup>\*,\*\*</sup>

Ondřej Procházka<sup>a,\*</sup>, Filip Novák<sup>a</sup>, Tomáš Báča<sup>a</sup>, Parakh M. Gupta<sup>a</sup>, Robert Pěnička<sup>a</sup> and Martin Saska<sup>a</sup>

<sup>a</sup>Czech Technical University in Prague, Faculty of Electrical Engineering, Czechia

## ARTICLE INFO

### Keywords:

Model Predictive Control  
Unmanned Surface Vehicle  
Unmanned Aerial Vehicle  
Multi-robot Systems  
Landing  
Harsh environment

## ABSTRACT

This paper proposes a novel trajectory generation method based on Model Predictive Control (MPC) for agile landing of an Unmanned Aerial Vehicle (UAV) onto an Unmanned Surface Vehicle (USV)'s deck in harsh conditions. The trajectory generation exploits the state predictions of the USV to create periodically updated trajectories for a multirotor UAV to precisely land on the deck of a moving USV even in cases where the deck's inclination is continuously changing. We use an MPC-based scheme to create trajectories that consider both the UAV dynamics and the predicted states of the USV up to the first derivative of position and orientation. Compared to existing approaches, our method dynamically modifies the penalization matrices to precisely follow the corresponding states with respect to the flight phase. Especially during the landing maneuver, the UAV synchronizes attitude with the USV's, allowing for fast landing on a tilted deck. Simulations show the method's reliability in various sea conditions up to *Rough sea* (wave height 4 m), outperforming state-of-the-art methods in landing speed and accuracy, with twice the precision on average. Finally, real-world experiments validate the simulation results, demonstrating robust landings on a moving USV, while all computations are performed in real-time onboard the UAV.

## 1. INTRODUCTION

There has been a significant increase in the utilization of Unmanned Aerial Vehicles (UAVs) in various domains in recent years, including tasks above water surfaces. UAVs have proven beneficial in marine wildlife monitoring Fortuna, Ferreira, Gomes, Ferreira and Sousa (2013); Yang, Yu, Dedman, Rosso, Zhu, Yang, Xia, Tian, Zhang and Wang (2022), search and rescue operations Doherty and Rudol (2007), and offshore safety monitoring to identify swimmers in distress Sharma, Saqib, Scully-Power and Blumenstein (2022). Moreover, UAVs can be deployed to detect garbage on the water surface Li, Huang, Wang, Yuan, Liu and Xu (2022). Individual garbage pieces can be then picked up by the drone itself, or its position can be shared from the UAV to the Unmanned Surface Vehicle (USV) for collection Akib, Tasnim, Biswas, Hashem, Rahman, Bhattacharjee and Fattah (2019). As it is clear, not only, from the aforementioned literature, the UAVs are a valuable resource for operations and study of maritime environments. However, their limited operation time necessitates a carrier ship to transport the UAV to the mission location for takeoff and

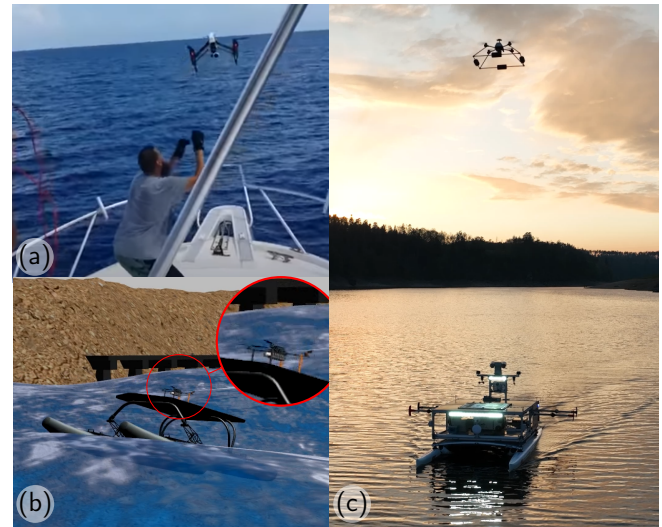


**Figure 1:** Motivation (a) manual landing of the UAV in the real world DailyPicksandFlicks (2016), (b) autonomous landing of the UAV in simulation in the high wave environment, and (c) photo of the UAV together with the USV research platform deployed in the real world.

landing in the vicinity of a mission area. The carrier ship brings the additional advantage of having better payload capacity and energy storage, and thus, can also be used to recharge the UAV Junaid, Konoiko, Zweiri, Sahinkaya and Seneviratne (2017). To maintain mission efficiency and eliminate the need for human intervention, the landing needs to be autonomous, which is challenging due to the severe conditions in a maritime environment. It is estimated that the probability of witnessing waves with a height of half a meter or more is approximately 90% worldwide Fossen

\* This work has been supported by the Technology Innovation Institute - Sole Proprietorship LLC, UAE, under the Research Project Contract No. TII/ARRC/2055/2021, CTU grant no SGS23/177/OHK3/3T/13 and the Czech Science Foundation (GAČR) under research project No. 23-06162M.

\*\* Multimedia materials: [https://mrs.fe1.cvut.cz/index.php?option=com\\_content&view=article&id=246](https://mrs.fe1.cvut.cz/index.php?option=com_content&view=article&id=246)

\*Corresponding author

[prochon4@fe1.cvut.cz](mailto:prochon4@fe1.cvut.cz) (O. Procházka)

<https://mrs.fe1.cvut.cz/members/phdstudents/ondrej-prochazka>

(O. Procházka)

ORCID(s): 0009-0009-2224-750X (O. Procházka); 0000-0003-3826-5904 (F. Novák); 0000-0001-9649-8277 (T. Báča); 0000-0002-6481-2281 (P.M. Gupta); 0000-0001-8549-4932 (R. Pěnička); 0000-0001-7106-3816 (M. Saska)

## Model predictive control-based trajectory generation for agile landing of unmanned aerial vehicle on a moving boat

(2011). Waves affect ship's position, altitude, attitude, and velocity such that the USV is sliding, tilting, and heaving simultaneously, making UAV landings challenging, especially on small USVs, preventing the use of standard landing maneuvers. Available mission time is further diminished by the time required for a visual search of the USV for landing, and additionally, for a collaborative mission (e.g. collaborative object manipulation on the water surface Novák, Báča and Saska (2024)), it is reasonable to assume that communication exists between the two vehicles. Therefore, this communication link is used to also share the position of the USV, allowing for a direct and time-efficient approach to the location of the USV. At the same time, we aim to shorten the landing maneuver itself as much as possible. While possibly dangerous in harsh sea conditions, the direct return to USV and the agile landing can significantly prolong the time for the main mission objectives.

This paper introduces a novel approach that enables UAVs to land autonomously on a moving or rocking USV in harsh environments utilizing a Model Predictive Control (MPC)-based trajectory generation in the process. This removes human intervention (see Figure 1) and increases the safety and reliability of the UAV's usage on the high seas. The proposed method relies on accurate estimation and prediction of USV's states, including position, rotation, and their first derivative, which are obtained from multiple sources to allow for landing in low visibility or harsh sea conditions Novak, Baca, Prochazka and Saska (2024). In contrast to our approach, most of the state-of-the-art methods Xu, Hu, Liu, Wang and Zhang (2020); Abujoub (2019); Venugopalan, Taher and Barbastathis (2012); Polvara, Sharma, Wan, Manning and Sutton (2018); Keller and Ben-Moshe (2022); Persson and Wahlberg (2019) rely on simplified models of the USV, which does not guarantee precise estimation of the USV's states. Consequently, landing accuracy in harsh environments cannot be assured due to the missing information about the USV's movement, which could result in an unsafe procedure or even a crash. To this end, our trajectory generator incorporates significantly more information about the USV state that is available during the individual phases of the UAV's operation and adjusts penalization matrices' values that prioritize specific states for tracking. The information about roll, pitch, yaw, linear movements, and Euler rates is taken into account to increase precision and reduce the harshness of the touchdown. This enables a significant increase in the performance of landings in various sea conditions and even on an inclined USV deck.

The simulation results demonstrate the proposed system's reliable performance in landing the UAV on a small scale USV under *Moderate sea* and even *Rough sea* conditions in which the height of the waves reaches up to 4 m. The system underwent extensive testing in more than 1,000 simulation experiments and was compared to the latest state-of-the-art work Gupta, Pairet, Nascimento and Saska (2022). We show approximately two times better touchdown accuracy with a 50 % faster landing maneuver on average. It is worth mentioning that our method achieved a success rate

of 100 % in most tested environment setups of the different sea conditions, with only two particularly challenging setups showing a slightly lower success rate, resulting in aborted and repeated landing. Moreover, the system was repeatedly tested in a real-world environment where its robustness and performance indicated in simulations were confirmed.

## 2. RELATED WORKS

Landing on a rocking and heaving platform, especially on a marine vessel in bad weather conditions, is a very challenging maneuver in which the helicopter can crash into the vessel or fall from the deck into the water. Even highly trained military pilots have difficulty with such a maneuver and thus rely on the visualization of horizon reference Stingl (1970) or use beartrap for a safer landing. Since it is impossible to use beartrap for small UAVs, the authors in Xu, Liu, Cao, Wang and Qian (2024) proposed a manipulator-assisted landing system that captures the hovering UAVs using the tethered connection. The landing is done on a USV's motion compensation platform, which is unlike the platform mentioned in the work of Tian, Li, Liao and Cao (2024) capable of compensating pitch and roll motions of the USV. The presented systems require a multiple-joint manipulator placed on the USV, and even so, for the UAV's position control, visual servoing feedback is used.

The visual servoing approaches can be divided into two categories: Position-Based visual servoing (PBVS) and Image-Based Visual Servoing (IBVS) Yang, Liu, Wang, Wang, Hu and Xi (2021). The PBVS method works in Cartesian space, whereas the IBVS approach works directly with the image input from sensors. The IBVS suffers from camera calibration errors, although the PBVS may suffer from position estimation errors. Moreover, it is noteworthy that the IBVS method Yang et al. (2021) assumes that the UAV's attitude changes are small, and can thus be neglected. Furthermore, the IBVS method uses a prediction of the landing zone for smoother control by using a Kalman filter Kalman (1960). The solution described in Yang et al. (2021) was tested on a simulated USV deck in the real world, proving that the UAV can detect and land on a tilting deck. Also, the dynamic landing algorithm presented in Ding and Huang (2023), which enables landing on the heaving USV, was tested in real-world scenarios. However, the authors do not present the roll and pitch tracking results upon the touchdown when USV is rocking.

The PBVS based on Proportional-Integral-Derivative (PID) controller introduced in Xu et al. (2020) was used for vision-based autonomous landing on a boat where an AprilTag Olson (2011) was placed on the helipad. The visual slide landing is suitable in a situation where it is not possible to hover above the helipad and perform a regular landing because of sails or cables Keller and Ben-Moshe (2022). Another work demonstrating the capability of landing on a one-direction fast-moving platform is presented in Zhang, Wu and Wei (2024). These landing approaches mostly do not model the USV's roll, pitch, and heave motions.

## Model predictive control-based trajectory generation for agile landing of unmanned aerial vehicle on a moving boat

The aforementioned visual-based approaches do not work well in limited lighting conditions. To enable landing at night, the marine vessel's deck can be equipped with infrared markers Meng, Wang, Han and Ban (2019) that are used to navigate fixed-wing aircraft to the runway during autonomous landing. Other approaches equip the UAV with Light Detection and Ranging (LiDAR) sensors Abujoub, McPhee and Irani (2020); Abujoub, McPhee, Westin and Irani (2018). LiDAR can detect the vessel's movements and use it for the Signal Prediction Algorithm (SPA) Abujoub et al. (2018). This algorithm includes mode detection, estimation, and prediction using Fast Fourier Transformation to identify the frequency, amplitude, and phase of the roll and pitch movements. Another approach that can determine a proper time for landing is based on estimating the ship's energy using Landing Period Indicator (LPI), where the pertinent motions are roll, pitch, and heave Abujoub et al. (2020). Regarding the vertical oscillations, the Active Heave Compensation (AHC) algorithm is proposed in the same paper Abujoub et al. (2020). The approach of the AHC algorithm is to stabilize the UAV over the deck to ensure a landing that considers the raising and lowering of the deck. Therefore, it can be used together with SPA or LPI.

The drawback of the methods mentioned above is that they are purely vision-based. As such, if the vessel is not in the Field of View (FOV) of the UAV's sensors, the global position of the USV is unknown. The UAV must find the USV by searching the area, which is an energy-consuming procedure. Furthermore, it is anticipated that cooperation between the UAV and USV will be required for certain mission tasks, and therefore the USV is expected to be in the vicinity of the UAV. A wireless communication between the UAV and the USV for sharing the global position of the USV is presented in Venugopalan et al. (2012); Paris, Lopez and How (2020). Nevertheless, it is shown that the Global Navigation Satellite System (GNSS) precision is not sufficient for small UAVs and mainly for the altitude estimation. Due to the potential unreliability and imprecision of GNSS, we rely on a method that combines UAV onboard vision-based sensors with USV onboard sensors to accurately estimate the states of the USV Novak et al. (2024). The method proposed in Novak et al. (2024) utilizes data from the USV's GNSS for a rough estimation of its location and incorporates visual relative localization system UltraViolet Direction And Ranging (UVDAR) Walter, Saska and Franchi (2018) and visual fiducial system AprilTag Wang and Olson (2016). Thanks to the UVDAR system, localization of the USV can be done even in reduced visibility conditions, such as evening or night. To enhance the precision of the USV's orientation and angular rate estimation and prediction during the landing maneuver, data from the USV's Inertial Measurement Unit (IMU) is used.

To increase the precision of the UAV's control algorithm, the PID controller is nowadays being replaced by a method referred to as MPC. This is also known as receding horizon control or moving horizon control García, Prett and Morari (1989); Rawlings (2000). In Ngo and Sultan (2014),

**Table 1**

Comparison of the aspects of landing approaches for the vessels in related research works.

Work	Dp <sup>1</sup>	Al <sup>2</sup>	Hc <sup>3</sup>	6-DOFs USV model	Real-world deployment
(1)	X	X	X	X	✓
(2)	X	X	✓	✓	X
(3)	X	X	X	X	X
(4)	X	✓	✓	X	✓
(5)	X	X	✓	✓	X
(6)	X	X	X	X	✓
(7)	X	X	X	X	X
(8)	X	X	X	X	✓
(9)	X	X	✓	✓	✓
(10)	X	✓	✓	✓	✓
(11)	X	✓	✓	✓	X
<b>This work</b>	✓	✓	✓	✓	✓

- (1) Venugopalan et al. (2012), (2) Ngo and Sultan (2014), (3) Polvara et al. (2018), (4) Persson and Wahlberg (2019), (5) Abujoub et al. (2020), (6) Xu et al. (2020), (7) Yang et al. (2021), (8) Keller and Ben-Moshe (2022), (9) Gupta et al. (2022), (10) Ding and Huang (2023), (11) Stephenson, Duncan and Greeff (2024)

<sup>1</sup> Dynamic adjustments of the penalization matrices to achieve better tracking of the individual USV's states during the flight and especially during the final touchdown.

<sup>2</sup> UAV aligns its position and orientation up to the first derivative with USV's upon touchdown.

<sup>3</sup> Heave motion compensation.

nonlinear MPC is used to control the landing of a helicopter on a navy vessel based on a prediction of the quiescent periods, which is made based on long-term observation of the USV's movements. This system was outperformed by methods presented in Gupta et al. (2022); Stephenson et al. (2024). Both methods use the same approach for a landing procedure, waiting for a low tilt of the USV. The landing maneuver is performed based on the defined internal landing cost function incorporated into the MPC, which penalizes the USV's rocking movements. Both Ngo and Sultan (2014); Gupta et al. (2022) landing approaches may require a long time for safe landing. Considering the limited flight time of UAVs, it is crucial to optimize the landing maneuver and shorten the overall return-to-home procedure. Thus, the maximum flight time can be used for the UAV's primary task (e.g., off-shore infrastructure inspection, oil spill monitoring, marine life tracking, and vessel inspection). However, these approaches Ngo and Sultan (2014); Gupta et al. (2022) need to wait for the USV's deck to be fully leveled or for calmness in wave motion, assuming that the surge and sway motions of the USV are negligible.

In the proposed approach, the UAV compensates the USV's attitude by synchronizing the UAV's attitude with the USV's, allowing for fast landing on a tilted deck. Furthermore, USV model, which is used, includes wave modeling that we introduced in Novak et al. (2024), contrasting with the state-of-the-art approaches, where such information is not considered. The model of the waves is crucial for

## Model predictive control-based trajectory generation for agile landing of unmanned aerial vehicle on a moving boat

heave motion estimation Reis, Batista, Oliveira and Silvestre (2023) and prediction. Such possible heave compensation integrated in the landing technique ensures low impact velocity during touchdown. These features make it usable in varying sea conditions and more efficient for safe and fast mission completion, even on *Rough sea*. A comparison summary of our proposed system with existing state-of-the-art approaches is shown in Table 1. According to this table, many works utilize the full 6 degrees of freedom (DOFs) USV model, heave motion compensation, and take into account USV's attitude angles. While many approaches have been tested in real-world scenarios, none incorporate dynamic penalization matrices adjustments to better track the USV's individual states during the final touchdown.

### 3. VEHICLES' MODELS

This section introduces the mathematical model and physics background of our work. The mathematical model of the USV serves as the basis for estimating and predicting USV's states. This section further comprises the derivation of the UAV's mathematical model, which is crucial for the subsequent MPC-based trajectory generation. To be able to describe the models, let us define the local East North Up (ENU) coordinate frame  $\mathcal{W}$  together with the UAV's body coordinate frame ( $C$ ) and USV's coordinate frame ( $\mathcal{B}$ ) as shown in Figure 2.

The precise modeling of the USV is crucial for accurate estimation and prediction of its states, which are essential conditions for designing a safe and accurate landing maneuver. For this purpose, the 6 DOF model of the USV utilized in

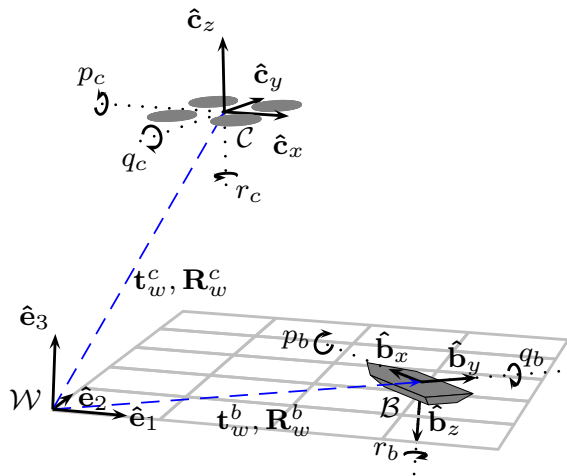


**Figure 2:** Illustration of the UAV's and USV's coordinate systems, where  $\mathcal{W}$  represents local ENU frame,  $C$  denotes the multicopter's body-fixed frame, and  $\mathcal{B}$  symbolizes the USV's body-fixed frame. The rotation matrix from the world frame to the USV's body-fixed frame is represented as  $\mathbf{R}_w^b$ , and the translation vector is denoted as  $\mathbf{t}_w^b$ . The rotation matrix  $\mathbf{R}_w^c$  and translation vector  $\mathbf{t}_w^c$  denotes rotation and translation from the world frame to the UAV's body-fixed frame. The angular velocity of the UAV and USV is denoted with  $(p, q, r)$  with the appropriate subscripts.

this work is composed of the standard Fossen's USV model Fossen (2002) and model of the waves as is proposed in Novak et al. (2024). According to Novak et al. (2024), the general definition of the USV model looks as follows

$$\dot{\boldsymbol{\eta}}_L = \mathbf{v}, \quad (1)$$

$$\dot{\mathbf{v}} = -\mathbf{M}^{-1}(\mathbf{D}\mathbf{v} + \mathbf{G}\boldsymbol{\eta}_L) + \mathbf{C}_{\text{wave},\mathbf{v}}\mathbf{x}_{\text{wave},\mathbf{v}}, \quad (2)$$

$$\dot{\mathbf{x}}_{\text{wave},\mathbf{v}} = \mathbf{A}_{\text{wave},\mathbf{v}}\mathbf{x}_{\text{wave},\mathbf{v}}, \quad (3)$$

where  $\boldsymbol{\eta}_L = [\hat{b}_x, \hat{b}_y, \hat{b}_z, \phi_b, \theta_b, \psi_b]^\top \in \mathbb{R}^3 \times \mathcal{S}^3$  is a vector composed of positions and orientations in *Vessel parallel coordinate system* Fossen (2011). Euler angles are  $\phi_b, \theta_b$ , and  $\psi_b$ ,  $\mathbf{v} = [u_b, v_b, w_b, p_b, q_b, r_b]^\top \in \mathbb{R}^6$  is a vector that contains the linear and angular speeds for all axes.  $\mathbf{G}$  represents matrix of gravitational and buoyancy forces,  $\mathbf{D}$  describes the system's damping,  $\mathbf{M} = \mathbf{M}_{RB} + \mathbf{M}_A$  is a sum of the USV's body inertia matrix and hydrodynamics inertia matrix. State-space representation matrix of the waves' damping and frequency is denoted with  $\mathbf{A}_{\text{wave},\mathbf{v}}$ . Matrix  $\mathbf{C}_{\text{wave},\mathbf{v}}$  is the diagonal output matrix of the size, which corresponds to the number of modeled waves, and  $\mathbf{x}_{\text{wave},\mathbf{v}}$  is the state vector, including all states of the individual waves components. Notice the model (1)–(3) is used solely for USV state estimation and prediction onboard the UAV, maintaining precision even in challenging conditions without relying on inputs like rudder and propellers, which would reduce robustness by increasing reliance on communication stability.

Based on the already formulated USV's model, the full nonlinear model of the UAV is defined as a rigid body model in three-dimensional space. Generalized positions (4) and velocities (5) are designated as

$$\boldsymbol{\eta}_c = [\boldsymbol{\eta}_{p_c}^\top, \boldsymbol{\eta}_{o_c}^\top]^\top = [\hat{c}_x, \hat{c}_y, \hat{c}_z, \phi_c, \theta_c, \psi_c]^\top \in \mathbb{R}^3 \times \mathcal{S}^3, \quad (4)$$

$$\mathbf{v}_c = [\mathbf{v}_l^\top, \mathbf{v}_a^\top]^\top = [v_x, v_y, v_z, v_\phi, v_\theta, v_\psi]^\top \in \mathbb{R}^6, \quad (5)$$

where vector  $\boldsymbol{\eta}_c$  is composed of position  $\boldsymbol{\eta}_{p_c} = [\hat{c}_x, \hat{c}_y, \hat{c}_z]^\top$  and orientation  $\boldsymbol{\eta}_{o_c} = [\phi_c, \theta_c, \psi_c]^\top$ . The Euler angles are described in intrinsic *zyx*-convention. The vector  $\mathbf{v}_c$  includes linear velocity  $\mathbf{v}_l = [v_x, v_y, v_z]^\top$  and the Euler rate vector  $\mathbf{v}_a = [v_\phi, v_\theta, v_\psi]^\top$ . The position  $\boldsymbol{\eta}_c$  and velocity  $\mathbf{v}_c$  are defined in the local ENU coordinate frame  $\mathcal{W}$ .

The translational dynamics of the UAV is defined as

$$\dot{\boldsymbol{\eta}}_{p_c} = \mathbf{v}_l, \quad (6)$$

$$\ddot{\boldsymbol{\eta}}_{p_c} = -g\hat{\mathbf{e}}_3 + \mathbf{R}_c^w \frac{\mathbf{T}_C}{m}, \quad (7)$$

where  $g$  denotes gravitation acceleration,  $\hat{\mathbf{e}}_3$  is an element of the *standard basis*, and  $m$  is the quadcopter weight. The  $\mathbf{R}_c^w$  is an intrinsic *xyz*-convention Euler rotation matrix. The total force (thrust)  $\mathbf{T}_C$  is generated in the body-fixed frame as

$$\mathbf{T}_C = [0 \quad 0 \quad k_T \sum_{i=1}^4 \omega_i^2]^\top, \quad (8)$$

where  $k_T$  is a lift constant for a motor with a propeller and  $\omega_i$  is the rotor's angular velocity. The angular dynamics in local coordinate frame  $\mathcal{W}$  are defined as

$$\dot{\boldsymbol{\eta}}_{o_c} = \mathbf{v}_a, \quad (9)$$

$$\ddot{\boldsymbol{\eta}}_{o_c} = (\mathbf{T}_c^w \mathbf{I}_c \mathbf{T}_w^c)^{-1} (\boldsymbol{\tau}_C - \mathbf{C}_l \dot{\boldsymbol{\eta}}_{o_c}), \quad (10)$$

## Model predictive control-based trajectory generation for agile landing of unmanned aerial vehicle on a moving boat

where  $\mathbf{C}_t$  is the Coriolis term, which contains centripetal and gyroscopic terms, as shown in Raffo, Ortega and Rubio (2010). The  $\boldsymbol{\tau}_c$  stands for the total torque generated by the rotors and  $\mathbf{I}_c \in \mathbb{R}^{3 \times 3}$  is an inertial matrix composed of  $I_{xx}, I_{yy}, I_{zz}$  on its diagonal. As shown in Jalón (2014), the transformation matrix  $\mathbf{T}_w^c = (\mathbf{T}_c^w)^T$  is defined as

$$\mathbf{T}_w^c = \mathbf{R}_{x,\phi_c}^T \mathbf{R}_{y,\theta_c}^T \mathbf{R}_{z,\psi_c}^T \hat{\mathbf{e}}_3 + \mathbf{R}_{x,\phi_c}^T \mathbf{R}_{y,\theta_c}^T \hat{\mathbf{e}}_2 + \mathbf{R}_{x,\phi_c}^T \hat{\mathbf{e}}_1, \quad (11)$$

where  $\hat{\mathbf{e}}_1, \hat{\mathbf{e}}_2, \hat{\mathbf{e}}_3$  are elements of the *standard basis*. It is also worth mentioning that the inversion  $\mathbf{T}_c^w$  of  $\mathbf{T}_w^c$  from (11) is not defined for  $\theta_c = \frac{\pi}{2} + j\pi, j \in \mathbb{Z}$ .

In order to provide the linear approximation of the equations of motion that were shown in (6), (7), (9), and (10), an equilibrium point is needed da Cunha (2015). We consider as equilibrium the hovering state of the UAV, which is defined as a state with zero derivatives of position. Thus, the linearized solution is introduced as

$$\begin{bmatrix} \dot{\eta}_{p_c} \\ \dot{\eta}_{o_c} \\ \dot{\eta}_{p_c} \\ \dot{\eta}_{o_c} \end{bmatrix} = \underbrace{\begin{bmatrix} \mathbf{0}^{6 \times 3} & \mathbf{0}^{6 \times 3} & \mathbf{I}^{6 \times 6} \\ \mathbf{0}^{6 \times 3} & \mathbf{A}_p & \mathbf{0}^{6 \times 6} \end{bmatrix}}_{\mathbf{A}_c} \begin{bmatrix} \eta_{p_c} \\ \eta_{o_c} \\ \dot{\eta}_{p_c} \\ \dot{\eta}_{o_c} \end{bmatrix} + \underbrace{\begin{bmatrix} \mathbf{0}^{8 \times 4} \\ \mathbf{B}_p \end{bmatrix}}_{\mathbf{B}_c} \begin{bmatrix} \omega_1^2 \\ \omega_2^2 \\ \omega_3^2 \\ \omega_4^2 \end{bmatrix}, \quad (12)$$

where  $\mathbf{A}_p$  is a sparse matrix which contains nonzero elements located at specific positions as follows

$$\mathbf{A}_p^{[1,2]} = \frac{k_T(\omega_{h_1}^2 + \omega_{h_2}^2 + \omega_{h_3}^2 + \omega_{h_4}^2)}{m}, \quad (13)$$

$$\mathbf{A}_p^{[2,1]} = \frac{-k_T(\omega_{h_1}^2 + \omega_{h_2}^2 + \omega_{h_3}^2 + \omega_{h_4}^2)}{m}, \quad (14)$$

$$\mathbf{A}_p^{[4,2]} = \frac{-b(\omega_{h_1}^2 - \omega_{h_2}^2 + \omega_{h_3}^2 - \omega_{h_4}^2)}{I_{zz}}, \quad (15)$$

$$\mathbf{A}_p^{[5,1]} = \frac{(I_{yy}b - I_{zz}b)(\omega_{h_1}^2 - \omega_{h_2}^2 + \omega_{h_3}^2 - \omega_{h_4}^2)}{I_{yy}I_{zz}}, \quad (16)$$

$$\mathbf{A}_p^{[6,1]} = \frac{(I_{yy}k_Tl - I_{zz}k_Tl)(\omega_{h_1}^2 - \omega_{h_2}^2 - \omega_{h_3}^2 + \omega_{h_4}^2)}{I_{yy}I_{zz}}, \quad (17)$$

$$\mathbf{A}_p^{[6,2]} = \frac{-I_{yy}k_Tl(\omega_{h_1}^2 + \omega_{h_2}^2 - \omega_{h_3}^2 - \omega_{h_4}^2)}{I_{yy}I_{zz}}, \quad (18)$$

where  $b$  is the drag constant of the motor with a propeller. Matrix  $\mathbf{B}_p$  is defined as

$$\mathbf{B}_p = \begin{bmatrix} \frac{k_T}{m} & \frac{k_T}{m} & \frac{k_T}{m} & \frac{k_T}{m} \\ -k_Tl & -k_Tl & k_Tl & k_Tl \\ \frac{I_{xx}}{-k_Tl} & \frac{I_{xx}}{k_Tl} & \frac{I_{xx}}{k_Tl} & \frac{I_{xx}}{-k_Tl} \\ \frac{I_{yy}}{-b} & \frac{I_{yy}}{b} & \frac{I_{yy}}{-b} & \frac{I_{yy}}{b} \\ \frac{I_{zz}}{-b} & \frac{I_{zz}}{b} & \frac{I_{zz}}{-b} & \frac{I_{zz}}{b} \end{bmatrix}. \quad (19)$$

We assume a symmetric X-shape of the UAV with arm length  $l$ . Variable  $\omega_{h_i}$  is the rotor's angular velocity in hover, which is equal to

$$k_T \sum_{i=1}^4 \omega_{h_i}^2 = mg. \quad (20)$$

Thanks to the linearized model of the UAV, it is possible to utilize linear MPC in the trajectory generation process, which is challenging due to the limitations of onboard computational power for searching the large solution space.

## 4. MPC-BASED LANDING TRAJECTORY GENERATION

In this section, we introduce the MPC-based trajectory generator designed specifically for landing a UAV on the tilting deck of a moving USV. Firstly, the derivation of the used MPC is detailed in Subsection 4.1. It is followed by Subsection 4.2 where the state machine responsible for determining the distinct flight mission phases, in which the UAV operates, is introduced. These stages of flight are used for MPC-based trajectory generator, which ensures that the generated trajectory will correspond to the specified flight stage e.g. approaching or landing maneuver. This assumption enables dynamically adjusting the defined problem during the process of trajectory generation both in terms of modifying MPC's objective and or its reference. Such a process is explained in Subsection 4.3.

### 4.1. Model Predictive Control

In general (see Rawlings (2000)), the objective function of the MPC in the tracking form is defined as

$$\min_{\mathbf{e}, \mathbf{u}} J(\mathbf{e}, \mathbf{u}) = \frac{1}{2} \mathbf{e}_{[t+N]}^T \mathbf{P} \mathbf{e}_{[t+N]} + \frac{1}{2} \sum_{k=1}^{N-1} \left( \mathbf{e}_{[t+k]}^T \mathbf{Q} \mathbf{e}_{[t+k]} + \mathbf{u}_{[t+k]}^T \mathbf{R} \mathbf{u}_{[t+k]} \right), \quad (21)$$

where  $k = \{1, \dots, N-1\}$  and  $N \in \mathbb{Z}^+$  is the size of the prediction and control horizon simultaneously,  $t$  stands for the current time, and  $\mathbf{e}_{[t+k]}$  denotes the error between the USV's states  $\mathbf{r}_{[t+k]}$  and the observable UAV's states  $\mathbf{y}_{[t+k]}$ . Both UAV and USV models were described in Section 3. The penalization matrices  $\mathbf{Q}$  and  $\mathbf{P}$  are diagonal positive semi-definite matrices. Usually, optimization problems are assumed to be time-invariant, eliminating the need for parameter modifications. However, in our case, it is highly beneficial to adjust the parameters of the matrix  $\mathbf{Q}$  based on the actual state of the flight, and therefore, from now onward we will assume the matrix to be  $\mathbf{Q}$  time varying  $\mathbf{Q}_{[t]}$ . For example, if the UAV is following the USV, the penalization of the UAV's and USV's linear velocity difference is increased. A detailed description is provided in the following sections. The weighting matrix  $\mathbf{R}$  is a diagonal positive-definite matrix that penalizes input signals  $\mathbf{u}$  in every control step, whereby this input corresponds to a vector containing the square of each rotor's individual angular velocities. The UAV's model (12), initial state, and both state and input constraints are defined as

$$\mathbf{x}_{[t+k+1]} = \mathbf{A} \mathbf{x}_{[t+k]} + \mathbf{B} \mathbf{u}_{[t+k]} \quad \forall k \in \{0, \dots, N-1\}, \quad (22)$$

$$\mathbf{x}_{[t]} = \text{measured current state}, \quad (23)$$

$$\mathbf{x}_{\min} \leq \mathbf{x}_{[t+k]} \leq \mathbf{x}_{\max} \quad \forall k \in \{1, \dots, N\}, \quad (24)$$

$$\mathbf{u}_{\min} \leq \mathbf{u}_{[t+k]} \leq \mathbf{u}_{\max} \quad \forall k \in \{1, \dots, N\}. \quad (25)$$

Assuming a steady state of the UAV in hover and having a tracking error close to zero, it is not possible to have a control input equal to zero. The objective function (21) tries to optimize the control input to reduce both the tracking error and the input itself during the optimization process, but it is not aware that the input should not be a nonzero value. This approach can increase the deviation between the desired and actual state, thus increasing the reference error. Therefore, the standard objective function (21) is reformulated. Instead of using the input signal  $\mathbf{u}_{[t+k]}$  itself, its increment is used:

$$\Delta \mathbf{u}_{[t]} = \mathbf{u}_{[t]} - \mathbf{u}_{[t-1]}. \quad (26)$$

This leads to the reformulation of a linear model, which must be augmented with the new state variable  $\mathbf{x}_{u[t-1]} \cong \mathbf{u}_{[t-1]}$  and the

## Model predictive control-based trajectory generation for agile landing of unmanned aerial vehicle on a moving boat

control input is exchanged for  $\Delta \mathbf{u}_{[t]}$ . The form of the augmented model is

$$\begin{bmatrix} \mathbf{x}_{[t+1]} \\ \mathbf{x}_{u[t+1]} \end{bmatrix} = \underbrace{\begin{bmatrix} \mathbf{A} & \mathbf{B} \\ \mathbf{0}^{m \times n} & \mathbf{I}^{m \times m} \end{bmatrix}}_{\mathbf{A}_a} \underbrace{\begin{bmatrix} \mathbf{x}_{[t]} \\ \mathbf{x}_{u[t]} \end{bmatrix}}_{\mathbf{x}_{a[t]}} + \underbrace{\begin{bmatrix} \mathbf{B} \\ \mathbf{I}^{m \times m} \end{bmatrix}}_{\mathbf{B}_a} \Delta \mathbf{u}_{[t]}, \quad (27)$$

$$\mathbf{y}_{[t]} = \underbrace{\begin{bmatrix} \mathbf{C} & \mathbf{0}^{p \times m} \end{bmatrix}}_{\mathbf{C}_a} \begin{bmatrix} \mathbf{x}_{[t]} \\ \mathbf{x}_{u[t]} \end{bmatrix}, \quad (28)$$

where  $\mathbf{x} \in \mathbb{R}^n$  is a state vector containing  $n$  states,  $\mathbf{u} \in \mathbb{R}^m$  is the control vector with  $m$  inputs, and  $\mathbf{y} \in \mathbb{R}^p$  is a system output vector. It is also assumed that the primary model omits direct feed-through of the input signal.

The objective function in its sequential form, incorporating an augmented model (27) – (28), and excluding constant terms (offsets that can be omitted without affecting the generality of the objective function) is derived by substituting  $\mathbf{e}_{[t]}$  with  $\mathbf{r}_{[t]} - \mathbf{C}_a \mathbf{x}_{a[t]}$  into (21) resulting in

$$\begin{aligned} \min_{\Delta \mathbf{u}} J(\Delta \mathbf{u}, \mathbf{x}_{[t]}, \mathbf{Q}_{[t]}) &= \frac{1}{2} \Delta \mathbf{u}^T (\bar{\mathbf{C}}_a^T \bar{\mathbf{Q}}_a \bar{\mathbf{C}}_a + \bar{\mathbf{R}}) \Delta \mathbf{u} + \\ &\begin{bmatrix} \mathbf{x}_{[t]}^T & \mathbf{u}_{[t-1]}^T & \mathbf{r}_{[t]}^T \end{bmatrix} \begin{bmatrix} \bar{\mathbf{A}}_a^T \bar{\mathbf{Q}}_a \bar{\mathbf{C}}_a \\ -\bar{\mathbf{T}} \mathbf{C}_a \end{bmatrix}^T \Delta \mathbf{u}. \end{aligned} \quad (29)$$

Matrix  $\bar{\mathbf{C}}_a$  denotes the controllability matrix of the augmented model of the UAV. Matrix  $\bar{\mathbf{A}}_a$  is a column matrix of the  $\mathbf{A}_a$  matrices of the length of the prediction horizon. Matrices  $\bar{\mathbf{Q}}$ ,  $\bar{\mathbf{T}}$  and  $\bar{\mathbf{R}}$  were obtained from a simplified simultaneous form of the objective function (21).

Since the objective function is introduced in sequential form, the constraints for the states are defined as

$$\bar{\mathbf{C}}_a \Delta \mathbf{u} \leq \mathbf{x}_{\max} - \bar{\mathbf{A}}_a \mathbf{x}_{a[t]}, \quad (30)$$

where  $\mathbf{x}_{\max} \in \mathbb{R}^{(n+m)N}$  are limiting values of the UAV state. This can be done accordingly for the lower bound. Also, slew rate constraints are added, which refer to the range of change of an input variable and are defined as

$$\Delta \mathbf{u}_{[t]} \leq \Delta \mathbf{u}_{\max}, \quad (31)$$

$$-\Delta \mathbf{u}_{[t]} \leq -\Delta \mathbf{u}_{\min}, \quad (32)$$

where  $\Delta \mathbf{u}_{\max} \in \mathbb{R}^{(m,N)}$  is a vector of the change of angular speed for individual propellers. The low-level formulation (29) allows us to use the whole linear model of the UAV and track position, attitude angles, linear velocities, and Euler rates while still being able to compute the problem in real-time. However, not all stages of the flight mission necessitate tracking all USV states. The forthcoming section introduces the mission and navigation state machine to address this aspect.

## 4.2. Mission and navigation

The UAV flight phases before landing are controlled by the finite state machine that actively changes what are the reference states for the MPC-based trajectory planning. The proposed state machine is designed to segment the operational mission, assuming the landing trajectory generator can initiate from any location near the USV, into several logical phases of flight. This segmentation aims to ensure safety and streamline the overall mission execution. We consider the UAV landing procedure to have three phases: NAVIGATION, FOLLOW, and LANDING. Individual phases are further divided into states, which are explained in the following paragraph and shown in Figure 3.

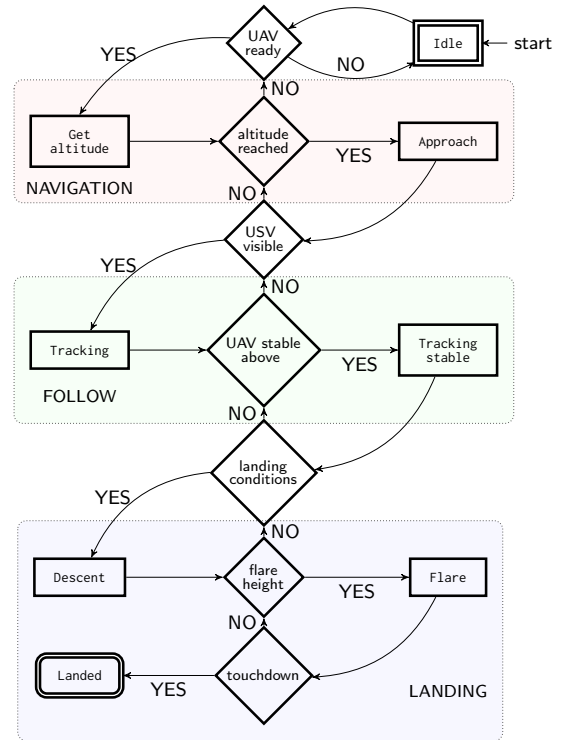


**Figure 3:** Illustration of the developed state machine composed of three phases ensures decision-making throughout the whole process.

1. The initial state is *Idle*. The UAV remains in this state until the landing command is initiated. If the UAV is flying and acquiring the USV's position using wireless communication, the state machine passes to the *NAVIGATION* phase.
2. *NAVIGATION* phase is composed of *Get altitude* and *Approach* states.
  - (a) In *Get altitude* state the UAV ascends or descends to a certain approach altitude.
  - (b) Then, the state machine transitions into the *Approach* state where the UAV's objective is to move to the USV's location, which is known thanks to the GNSS system and mutual communication. The UAV operates in this state up to the confirmation of visual contact of the USV when the USV's state prediction starts using visual relative localization systems instead of using GNSS, which can suffer from drifts. At that moment, the state machine passes to the next phase.
3. *FOLLOW* phase is composed of *Tracking* and *Tracking stable* states. The goal of this state is to follow the USV.
  - (a) The first state of the *FOLLOW* phase is *Tracking*, which represents the UAV's final approach above the USV's deck to the tracking altitude.
  - (b) When the UAV is above the deck at a predefined altitude, the state machine passes to *Tracking stable* and waits for the appropriate conditions for landing while the UAV is tracking the USV. These conditions are the distance threshold from the USV's center in the horizontal plane, the predicted trajectory of the USV must be feasible for the UAV, and the estimated USV's position covariance must be in a predefined limit. When all conditions for landing are met, the state machine passes to the next phase.

## Model predictive control-based trajectory generation for agile landing of unmanned aerial vehicle on a moving boat

4. LANDING phase is composed of Descent, Flare, and Landed states.
- The Descent state represents the initial stage of the landing maneuver in which the UAV starts descending towards the USV's deck. If one of the landing conditions is violated or the new measurements are not received within a predefined time limit, the state machine transitions to the state Tracking.
  - The previous state passes to the state Flare when the UAV reaches a certain height above the USV's deck. This maneuver is similar to an airplane's final stage of landing approach in which UAV tries to match the attitude with the USV's deck in order to land smoothly on all legs. The touchdown is verified by monitoring the estimation of the needed thrust to maintain the flight and verified using accelerometers and the range finder sensor. In case of missing the landing platform and losing sight of the USV's deck the UAV will return to the phase FOLLOW. For these emergency situations, the trajectory generator has the minimum altitude set which prevents generating the trajectory into the water.
  - After touching down, the UAV's motors are turned off and the state machine passes to the Landed state.

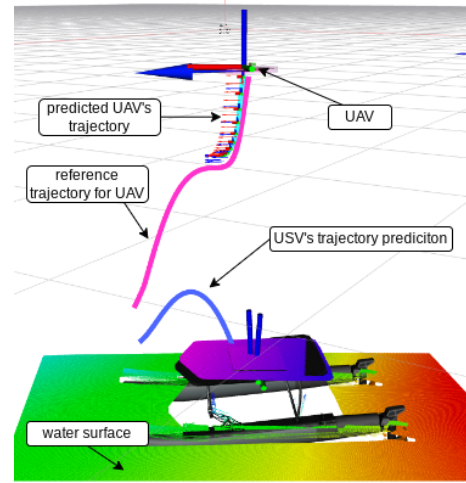
By dividing the landing problem into smaller individual states, it is possible to customize the MPC-based trajectory generation and the reference passed to the MPC for each state of flight.

### 4.3. Trajectory generation

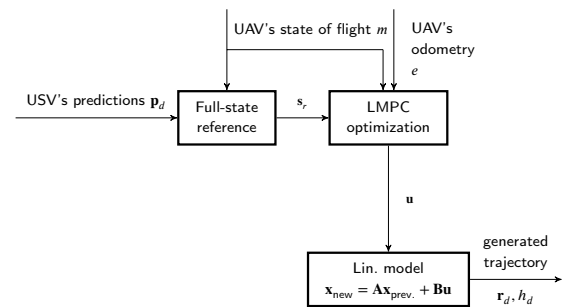
The MPC-based trajectory generation aims to create references for the UAV based on the UAV's flight phase. In the first phase of the UAV's operation (NAVIGATION), a point reference in the approach altitude  $h_a$  and directly above the current UAV's position is used. Moreover, the UAV's heading reference is adjusted, such that the camera on the UAV aims towards the USV's location. The predicted  $x, y$  coordinates of the USV are used for the Approach state. Hence, the trajectory from the MPC ensures that the control leads the UAV's position in such a way that the UAV performs an approach to the USV's position at a given approach altitude  $h_a$  and heading  $h$  directing towards the USV. Due to this, the camera can be mounted on the drone under a certain angle, enabling efficient use of the camera's FOV. For the FOLLOW phase, the predicted velocity of the USV is added to the reference. The UAV is thus able to follow the moving USV, maintaining the predefined altitude  $h_r$ .

During a descent maneuver, the reference is a trajectory generated by sampling the  $z$ -position to maintain a specific vertical approach velocity relative to the USV's deck. Additionally, a vertical velocity reference is established to maintain a constant mutual vertical speed. The visualization of such obtained guided path can be seen in Figure 4a. Throughout the flare maneuver, the predicted position, linear velocity, attitude angles, and Euler rates of the USV's deck are supplied to the *MPC optimization* (see Figure 4b) to create a trajectory that minimizes both position and attitude deviation upon the touchdown. Thanks to the continuous creation of the trajectory, the UAV can react to the latest USV state.

However, even when tracking all USV states during the final flare maneuver, it does not guarantee a smooth touchdown regarding attitude alignment. It is because of the fact that the UAV's horizontal acceleration is controlled by tilting, and therefore, change in roll and pitch angle influences the velocity and the position of the UAV, which is also demanded to be tracked as precisely as possible. To address this challenge, we propose a method that



(a) The visualization in Rviz illustrates the creation of the guiding path for the MPC-based trajectory generator, depicting the beginning of the landing maneuver.



(b) Diagram of the trajectory generator, where the UAV's flight state comes from the state machine and  $s_r$  is a modified full-state reference of the size of the prediction horizon that the MPC tracks. The MPC's output is a sequence of action interventions  $u$ , which are fed one by one into the linear model and from which the desired trajectory  $(r_d, h_d)$  is created.

**Figure 4:** Visualization of the landing maneuver in Rviz together with the trajectory generator pipeline diagram.

dynamically changes penalization matrix  $Q_{[t]}$  from (29) to get the most precise tracking of the certain states such as attitude angles upon the touchdown. For this purpose, we introduce an exponential function

$$f(v_d) = 1 + \frac{\alpha}{e^{\beta v_d}} \quad (33)$$

that is used to change the elements of the penalization matrix  $Q_{[t]}$ , specifically roll and pitch angles. This function depends on the vertical distance  $v_d$  between the UAV and the USV's deck. The coefficients  $\alpha$  and  $\beta$  are tuned to increase the value of the specific elements of the  $Q_{[t]}$  in sufficient distance to have time for the attitude synchronization maneuver, which we call Forcing Attitude Alignment (FAA). This can be done only when the approach velocity is constant, which was already achieved by adjusting the reference vertical speed, as mentioned above. As the UAV approaches the deck, the  $Q_{[t]}$ 's matrix weights belonging to the attitude angles exponentially increase, resulting in prioritizing the correction of attitude deviations over other tracked USV's states. It



## Model predictive control-based trajectory generation for agile landing of unmanned aerial vehicle on a moving boat

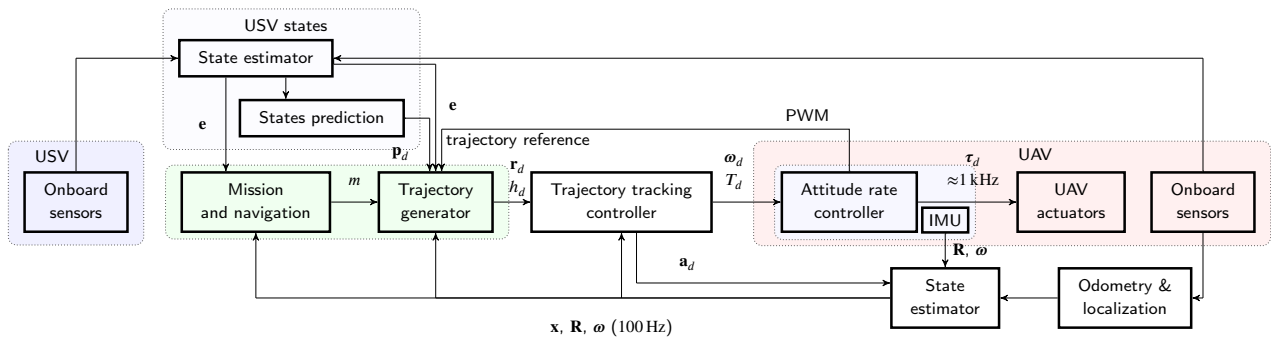


**Figure 5:** Full system pipeline diagram including USV's estimation/prediction, mission planning, trajectory planning, and the Multi-robot Systems multirotor control system Baca et al. (2021). *Mission and navigation* software supplies the flight mode ( $m$ ) to the *Trajectory generator* where the reference trajectory composed of headings and positions ( $\mathbf{r}_d, h_d$ ) is generated. *Trajectory tracking controller* ensures the trajectory is precisely tracked by producing the desired thrust and angular velocities ( $T_d, \omega_d$ ) for the Pixhawk embedded flight controller. The *State estimator* fuses data from *Onboard sensors* and *Odometry & localization* methods to create an estimate of the UAV translation and rotation ( $\mathbf{x}, \mathbf{R}$ ). Estimated states ( $\mathbf{e}$ ) and a full-states prediction ( $\mathbf{p}_d$ ) of the USV are provided by the *State estimator* and *States prediction* software, which exploits the *Onboard sensors* of the UAV and USV.

is also noteworthy that aligning the attitude is advantageous even when landing on a rapidly moving USV.

In the final stage of the MPC-based trajectory generator the MPC's output is not used directly, instead the trajectory is computed using angular rates of the individual motor obtained from MPC and UAV's linear model. The generated trajectory serves as the tracking trajectory for the *Reference tracker* in Multi-robot Systems (MRS) system Baca, Hert, Loiano, Saska and Kumar (2018). A graphical representation of the trajectory generator interconnection into the MRS UAV control system is shown in Figure 5.

## 5. SIMULATION VERIFICATION

The integration of the proposed method into the MRS system Baca et al. (2021); Hert, Baca, Petracek, Kratky, Penicka, Spurny, Petrlik, Vrba, Zaitlik, Stoudek et al. (2023) enabled realistic verification in a simulated environment, which allowed us to test the system under various conditions and even in high wind. The MRS system estimates the wind-based forces and deflections, which are then corrected by the attitude rate controller. As shown in Table 2, the most probable waves have a height between 1.25 m and 2.5 m. Therefore, we primarily focused on designing the overall system using the proposed method to efficiently land the UAV on the USV located in *Moderate sea*. In the first simulation experiment, the USV is left uncontrolled, drifting with the water current in Subsection 5.4. Then, the USV is following a predefined path in Subsection 5.5. Lastly, the proposed approach was compared to the most related state-of-the-art approach Gupta et al. (2022) in Subsection 5.6.

### 5.1. Simulation Environment

The proposed approach was thoroughly tested in a simulation with highly realistic waves that was inspired by the project called Virtual RobotX (VRX) Bingham, Agüero, McCarrin, Klamo, Malia, Allen, Lum, Rawson and Waqar (2019), which was created for the maritime VRX Competition. The designation of the waves together with their heights is denoted in Table 2. It is also worth mentioning that the height of the waves also correlates with wind speed, as shown in (Abujoub, 2019, p. 13). However, the wind is omitted in the simulations. The simulation environment based on

**Table 2**

Definition of sea state codes Bishop and Price (1974). Notice that the percentage probability for Calm and Smooth seas are summed up. The table is a modified version of the one from (Fossen, 2011, p. 200).

Description of sea	m Wave height observed	Percentage probability %		
		World wide	North Atlantic	Northern North Atlantic
Calm <sup>1</sup>	0			
Calm <sup>2</sup>	0–0.1	11.2486	8.3103	6.0616
Smooth <sup>3</sup>	0.1–0.5			
Slight	0.5–1.25	31.6851	28.1996	21.5683
Moderate	1.25–2.5	40.1944	42.0273	40.9915
Rough	2.5–4.0	12.8005	15.4435	21.2383
Very rough	4.0–6.0	3.0253	4.2938	7.0101
High	6.0–9.0	0.9263	1.4968	2.6931
Very high	9.0–14.0	0.1190	0.2263	0.4346
Phenomenal	Over 14.0	0.0009	0.0016	0.0035

<sup>1</sup> (1) glassy, (2) rippled, (3) wavelets

the MRS Gazebo simulation<sup>1</sup> was created (see Figure 6). The UAV, which was used in simulations, weights 3.5 kg, is 0.15 m in height and the arm length is 0.325 m. The USV is 5 m long, 2.5 m in width, 1.3 m in height and weights around 180 kg. Its landing platform, which measures 2.5 m in length and 1.7 m in width, is covered with the AprilTag with a side length of 1 m. The USV is equipped with an engine mounted on a joint at the back of each float, allowing it to navigate through predefined waypoints using a simple PID controller.

Water motion is modeled using the summation of Gerstner waves that represent the water surface as a trochoidal shape Tessendorf (2001). This allows to adjust the amplitude, period, direction, and steepness of the waves. The horizontal and vertical displacements of the wave-field to the undisturbed horizontal location  $\mathbf{x}_0 = [x_0, y_0]^T$  with a vertical height of  $\zeta_0 = 0$  are defined as

$$\mathbf{x}(\mathbf{x}_0, t) = \mathbf{x}_0 - \sum_{i=1}^{N_w} q_i (\mathbf{v}_i / v_i) A_i \sin(\mathbf{v}_i \mathbf{x}_0 - \omega_{w_i} t + \phi_i), \quad (34)$$

<sup>1</sup>[https://github.com/ctu-mrs/mrs\\_uav\\_gazebo\\_simulation](https://github.com/ctu-mrs/mrs_uav_gazebo_simulation)

## Model predictive control-based trajectory generation for agile landing of unmanned aerial vehicle on a moving boat

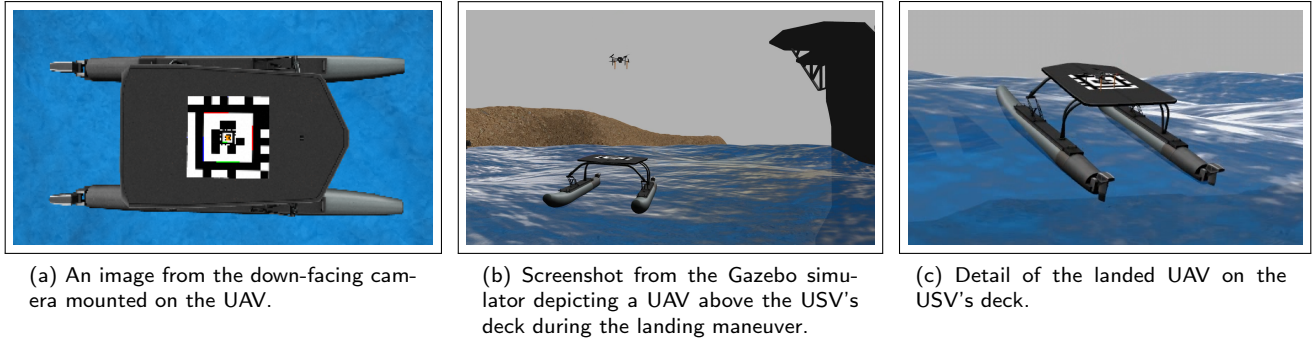


**Figure 6:** Screenshots from the Gazebo simulator during the UAV's landing maneuver on *Moderate sea*.

$$\zeta(\mathbf{x}_0, t) = \sum_{i=1}^N A_i \cos(\mathbf{v}_i \mathbf{x}_0 - \omega_{w_i} t + \phi_i). \quad (35)$$

Each wave component is defined with steepness  $q_i$ , amplitude  $A_i$ , angular frequency  $\omega_{w_i}$ , random phase  $\phi_i$ , and wave vector  $\mathbf{v}_i$  in the direction of travel with the magnitude of  $v_i$ . The  $N_w$  in (34) is the number of wave components at time  $t$ . In our case, three wave components  $N_w$  were used to simulate an offshore environment. It is also worth mentioning that waves with a steepness greater than 1:7 (wave height to wavelength) are considered breaking waves, which means that they are breaking at their crest Toffoli, Babanin, Onorato and Waseda (2010). Therefore, the nonbreaking waves can have a maximum inclination of around  $25^\circ$ . We assume that the UAV together with the USV will not be operated in worse conditions for safety reasons. This implies that the UAV's landing maneuver won't be performed in such conditions.

## 5.2. USV state estimation and prediction

The core component of the state estimation and prediction system is the Kalman filter, which fuses data from multiple sensors to increase the method's reliability. The system uses a mathematical model of the USV in the prediction step, which can provide temporary estimates even if no new sensory data are received for a limited time. The accuracy of predicted states depends on the accuracy of the USV model (see Section 3) and the correctness of its defining parameters, which specify the USV's properties. The potential imprecision of the model identification impacts the prediction of the USV states used by the trajectory generator, which can lead to an imprecise landing. The predicted USV states are position  $[\hat{b}_x, \hat{b}_y, \hat{b}_z]^\top$ , attitude  $[\phi_b, \theta_b, \psi_b]^\top$ , linear velocity  $[u_b, v_b, w_b]^\top$ , and Euler rates  $[p_b, q_b, r_b]^\top$ .

The state estimation system relies on mutual communication, sharing the GNSS location and IMU data. For precise localization during the FOLLOW and LANDING phases, visual relative localization is employed using the AprilTag detector and UVDAR system, and even the GNSS information can be utilized in extreme cases in these operational phases. Additionally, an IMU is employed for the attitude and angular velocity estimation. This phase heavily relies on the precision and noise levels of sensory measurements. Extensive verification of the used sensors, as detailed in Novak et al. (2024), indicates that the AprilTag detector delivers the lowest error in position and linear velocity estimation, whereas the IMU excels in attitude and Euler rates estimation. According to Novak et al. (2024), the estimation performance measured with Root Mean Square Error (RMSE) under *Moderate sea* conditions of the used estimation system is following. Position RMSE is equal to 0.116 m, attitude RMSE is 0.017 rad, linear velocity RMSE is 0.201 m s<sup>-1</sup> and angular velocity RMSE is 0.004 rad s<sup>-1</sup>.

**Table 3**

Trajectory generator settings and limits for trajectory state machine.

Symbol	Value	Description
$h_a$	15 m	approach altitude
$h_t$	7 m	tracking altitude
$v_{la}$	1 m s <sup>-1</sup>	landing approach velocity
$v_{fa}$	0.5 m s <sup>-1</sup>	flare approach velocity

## 5.3. MPC-based trajectory generation settings

The configuration of the MPC-based trajectory generator is based on the attributes of the employed UAV and our practical experiences. However, this does not limit our method to a specific type of UAV, as the UAV model presented in Section 3 was described in a general manner and therefore the mathematical model can be tailored to a specific UAV.

We summarize the most important parameters of our method, such as the altitude for approach state or vertical velocity in landing state in Table 3. These parameters were obtained empirically and can be changed dynamically at any time during the flight. We also put constraints on both the linear and angular velocities based on the limitations of the *Reference tracker*, as shown in the block diagram in Figure 5. These limits are listed in Table 4. These parameters can be adjusted according to the used UAV. However, it must be noted that if the limits are too low, the UAV may never perform a landing maneuver in harsh sea conditions. This is because the USV's movements may not be achievable by the UAV.

It was experimentally found that the maximum speed of the USV on which is our method capable of successfully landing is 7 m s<sup>-1</sup> in *Calm sea* environment. On the other hand, the same speed of the USV is not achievable in harsh sea conditions due to the acceleration limitations within which the state estimator is capable of providing an accurate estimation.

Another important parameter of the proposed method is the length of the generated trajectory. In this work, we use 2 s prediction horizon with 20 prediction steps. The length of the trajectory was determined based on the computation complexity. Our analysis showed that the trajectory generator can operate at a maximum frequency of 10 Hz, allowing sufficient time for the solver to converge in the NAVIGATION phase. During the FOLLOW and LANDING phases, the operation rate increases to 50 Hz since the solution is found within a maximum of 20 ms. The inconsistent computation time is handled by the MRS system trajectory tracker, which performs the interpolation of the given trajectory to find the correct time and state to follow and which ensures smooth tracking of a given trajectory.

## Model predictive control-based trajectory generation for agile landing of unmanned aerial vehicle on a moving boat

**Table 4**

Maximal allowed constraints for UAV model in trajectory generator to generate landing trajectories for the UAV and penalization matrices used in the objective function.

Symbol	Value	Description
$\mathbf{R}$	*blkdiag[0.1, 0.1, 0.1, 0.1]	control input weighting matrix
$\mathbf{Q}$	*blkdiag[30, 30, 40 + $\frac{10000}{e^{20d}}$ , 1 + $\frac{50000}{e^{10d}}$ , 1 + $\frac{50000}{e^{10d}}$ , 50, 1, 1, 3000 + $\frac{3000}{e^{25d}}$ , 1, 1, 1]	state weighting matrix
$\mathbf{P}$	*blkdiag[0, 0, 0, 0, 0, 0, 0, 0, 0, 0]	final state weighting matrix
$\phi, \theta$	$\pm 0.7854$ rad	roll and pitch min/max angle
$v_x, v_y$	$\pm 8$ m s <sup>-1</sup>	horizontal velocity in x and y axis
$v_z$	$\pm 4$ m s <sup>-1</sup>	vertical min/max velocity
$v_\phi, v_\theta, v_\psi$	$\pm 2$ rad s <sup>-1</sup>	roll, pitch and yaw rotation velocity

\* blkdiag denotes block diagonal matrix

#### 5.4. Landing on a USV carried by current

In the first set of experiments, the USV was located on a *Moderate sea* and was passively carried by the water current, which is a typical situation in many UAV-USV scenarios. Empirical findings indicate that setting the Gerstner wave's peak amplitude to 0.5 m and the period to 5 s resulted in waves with heights ranging from 0.6 m to 2.8 m in simulation. The position and heading were randomly generated within a predefined range for the experiments.

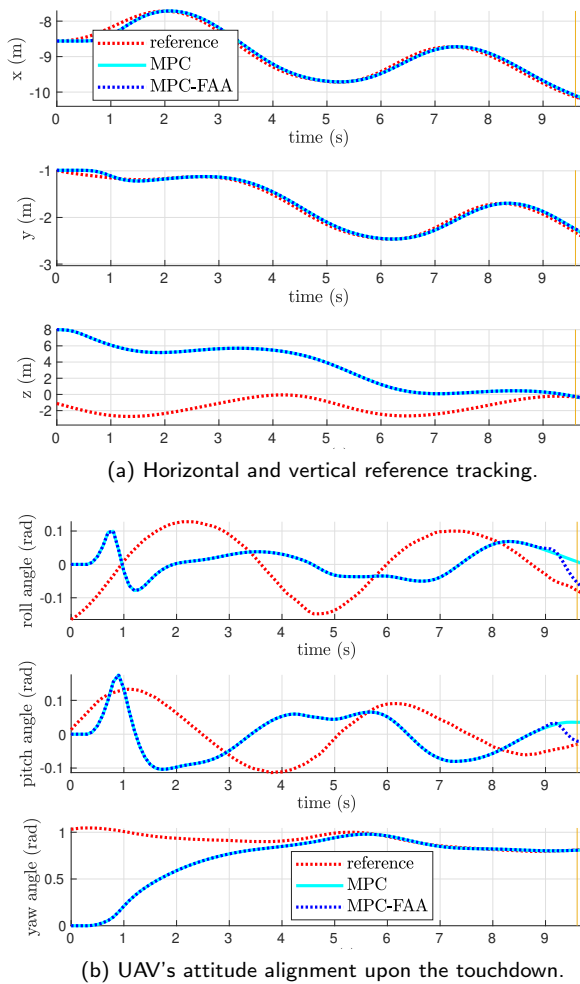


**Figure 7:** Comparison of the MPC-based trajectory generator with FAA at the final pre-touchdown maneuver and without FAA in simulation. The vertical yellow line indicates a touchdown.

The recorded motion of the USV was employed to fine-tune the  $\alpha$  and  $\beta$  coefficients from (33) for MPC-based trajectory generator using FAA. The comparison of MPC-based trajectory generator with and without FAA is demonstrated in Figure 7. The graphs show the UAV's horizontal and vertical position together with attitude-tracking reference and performed tracking of the UAV during the simulated landing maneuver. The trajectory generated by the MPC-based trajectory generator utilizing FAA ensured synchronization of attitude angles at the touchdown. In contrast, the MPC-based trajectory generator without FAA does not assure this synchronization. If we compare position precision while using FAA, the performed position deteriorated only 1 cm in the x-axis and 1.5 cm in the y-axis. This demonstrates that the FAA approach ensures better synchronization of the UAV's and USV's attitude angles upon the touchdown without any apparent deterioration in position precision.

Our approach was tested repeatedly in realistic real-world environment simulations. The takeoff position of the UAV was placed randomly, always at least 40 m away from the USV. The trajectories of both the UAV and USV from one of the experimental trials are depicted in Figure 8. The graphs show that the UAV ascended from the initial altitude  $Id_{1e}$  to the approach altitude. It then began approaching the USV's position at time 11 s and continued through all flight states, which are detailed in Subsection 4.2. The landing maneuver started at time 29 s and lasted approximately 6 s until the Flare state began. The touchdown was performed at time 35.5 s. This shows that the proposed method is capable of generating

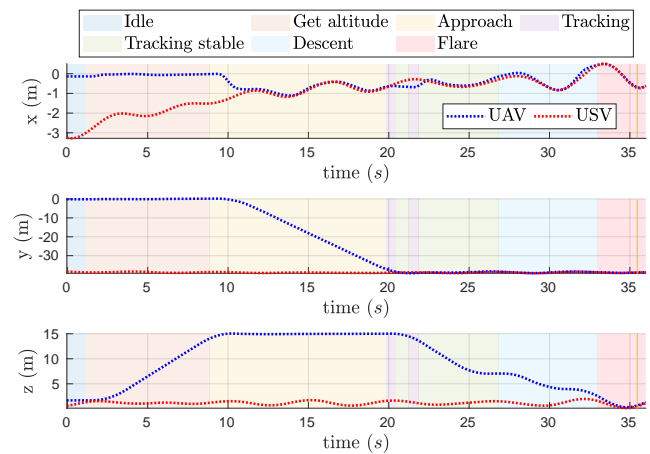


**Figure 8:** Comparison of the UAV and USV positions together with the state machine states during one of the experiments on *Moderate sea*. The vertical yellow line indicates a touchdown.

Model predictive control-based trajectory generation for agile landing of unmanned aerial vehicle on a moving boat

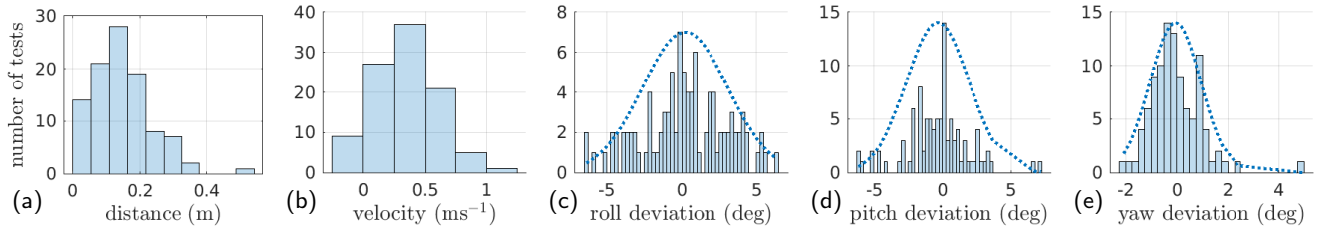


**Figure 9:** The assessment of the 100 UAV’s touchdowns on USV’s deck located in *Moderate sea* conditions using normal distribution analysis for evaluation of the (a) position deviation  $\mathcal{N}(0.15, 0.09^2)$ , (b) horizontal velocity deviation  $\mathcal{N}(0.36, 0.25^2)$ , (c) roll deviation  $\mathcal{N}(0.23, 2.85^2)$ , (d) pitch deviation  $\mathcal{N}(-0.32, 2.30^2)$  and (e) yaw deviation  $\mathcal{N}(-0.05, 0.99^2)$  during touchdown.

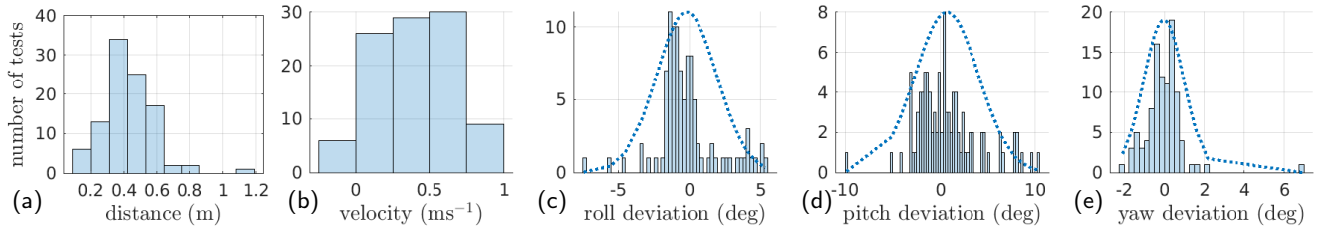


**Figure 10:** The results from 100 UAV touchdowns performed when the USV was following a path on *Slight/Moderate sea*. (a) Position deviation  $\mathcal{N}(0.44, 0.16^2)$ , (b) horizontal velocity deviation  $\mathcal{N}(0.41, 0.26^2)$ , (c) roll deviation  $\mathcal{N}(-0.14, 2.21^2)$ , (d) pitch deviation  $\mathcal{N}(0.59, 3.32^2)$  and yaw deviation  $\mathcal{N}(-0.02, 1.05^2)$  during touchdown.

trajectories that enable a fast approach and landing. Moreover, we show that our approach is able to land quickly within 6 seconds in waves with a height up to 2.5 m and on an inclined USV’s deck.

To demonstrate the reliability of our method, we ran 100 randomly initiated landing tests. The accuracy of the landing is of the utmost importance, as it must be accurate in order to land successfully within the landing zone of the size of a roughly 2 m x 2 m deck. A significant roll or pitch deviation between the USV and UAV can result in overturning the UAV, leading to potential damage and, thus, unsuccessful landing. On the other hand, maintaining the impact velocity within certain limits in order to prevent a strong impact with the USV’s deck is crucial.

Statistical results evaluating the touchdown’s precision, with normal distribution analysis, are depicted in Figure 9. The errors in position during the touchdown are shown in Figure 9a. The maximum displacement recorded in one of the one hundred experiments was 0.5 m, which is still considered as safe landing. All other experiments ended with a displacement smaller than 0.35 m. The impact speed of the UAV into the USV’s deck (see Figure 9b) is within limits for safe landing. The calculated velocity smaller than zero is caused by the inaccurate detection of the landing when the approach speed is close to zero. In 91 % of the landing experiments, the roll angle deviation was within  $\pm 5^\circ$ , and the pitch angle deviation did not exceed  $4^\circ$  in 90 % of cases as shown in Figure 9c and in Figure 9d. Yaw angle control demonstrated high accuracy, with deviations exceeding two degrees only three times during all touchdowns (see Figure 9e). Therefore, it is worth mentioning that the yaw angle outlier at  $4.75^\circ$  was most likely caused by the USV, which slightly rotated the UAV before the touchdown was detected.

### 5.5. USV following predefined path

The proposed method was designed to be able to plan landing trajectories such that the USV is not forced to stop or suspend its current task. Due to the increased complexity of landing on a moving boat, the simulated environment conditions were mitigated

to *Slight sea* and *Moderate sea* levels. Consequently, the average wave height was around 1.25 m.

One of the experiments in which the USV followed a square-shaped path at a speed of around  $2 \text{ m s}^{-1}$  is shown in Figure 11. The indicated velocity of the USV is for information only because it was measured under *Calm sea* conditions. However, in the tested sea conditions, the speed fluctuated due to the influence of waves. The experiment started with the UAV approximately 90 m away from the USV. The UAV was able to catch up with the USV at time 32 s and began descending into the Follow phase. At 38 s, as can be seen from the attached Figure 11, the USV changed its direction of motion. Nevertheless, all conditions for landing were met and the landing maneuver started almost immediately, continuing into the Flare state. The UAV landed at 45 s.

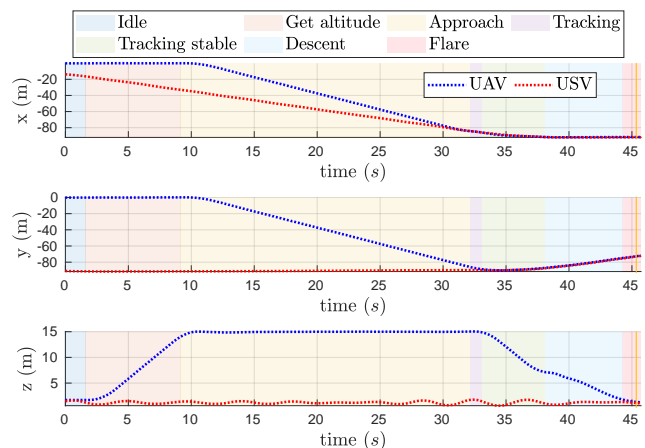


**Figure 11:** Comparison of the UAV and USV positions together with the state machine states, while the boat was following a predefined path at a speed of  $2 \text{ m s}^{-1}$ . The vertical yellow line indicates a touchdown.

## Model predictive control-based trajectory generation for agile landing of unmanned aerial vehicle on a moving boat

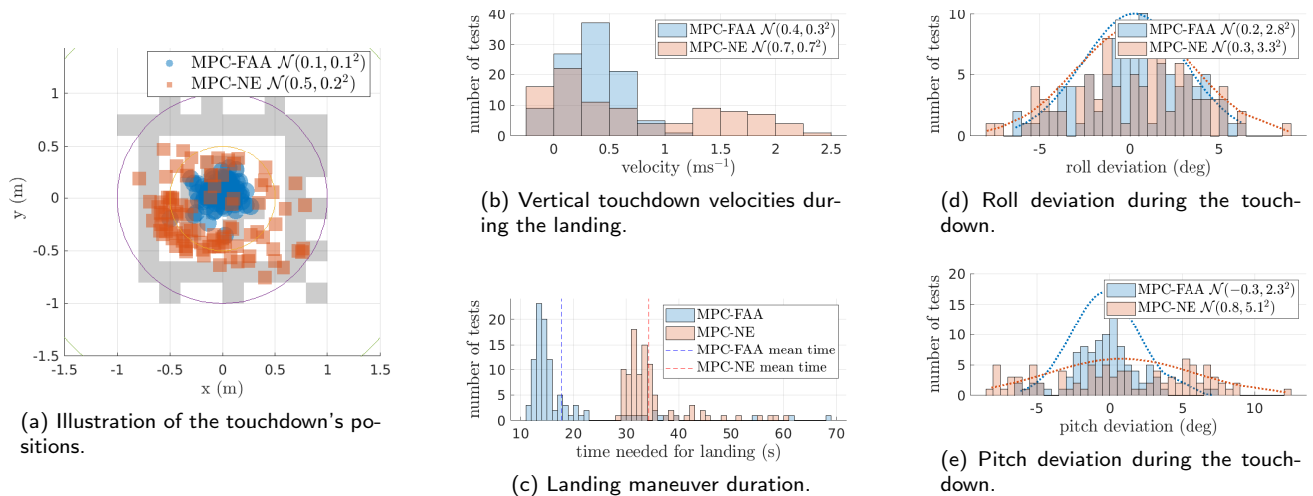


**Figure 12:** Comparison of the proposed MPC-FAA and MPC-NE methods in waves with a height of up to 2.5 m (*Moderate sea*).

The aforementioned experiment was conducted 100 times with 100 % success rate to gather statistical results (see Figure 10), showing slightly worse results compared to landing on a USV being carried by the current (Subsection 5.4). The measured deviations upon touchdown are higher here due to the increased accelerations experienced by the USV, resulting in a less accurate estimation of the USV's motions. The mean position error of touchdown increased from 15 cm to 0.44 m (see Figure 10a). On the other hand, the mean approach velocity increased only by  $0.05 \text{ m s}^{-1}$ , as can be seen in Figure 10b. The yaw's deviation mean value (Figure 10e) is close to zero, and most tests ended with a yaw deviation between  $\pm 2$  degrees. However, values larger than  $2^\circ$  also appeared, which was caused by the fact that some landing attempts were performed during the USV's turning maneuver, where the USV's yaw angle estimation was lagging slightly behind. The ability to align the roll and pitch angles upon the touchdown ensured that most of the touchdown attempts ended up close to the demanded attitude (see Figure 10c and Figure 10d, ensuring a safe touchdown.

## 5.6. Comparison with state of the art

According to our knowledge and based on the comprehensive state-of-the-art study (for the summary, see Table 1), we found as the most relevant work of Gupta et al. (2022). However, the method MPC-NE in Gupta et al. (2022) utilizes only the AprilTag measurements for the USV's position estimation and does not align the yaw angle of the UAV with the USV's. MPC-NE is not capable of the initial approach to the USV's position when the USV is not in the FOV of the UAV's camera. Therefore, the landing phase is the only part of our method MPC-FAA that can be compared with the state-of-the-art method MPC-NE.

More than one thousand simulations for each method were done to obtain the statistical results. The primary focus of interest while comparing both methods was the accuracy of the landing, specifically, the precision of position, attitude, and impact velocity. Another crucial parameter that was compared is the duration of the landing maneuver itself.

### 5.6.1. Comparison of landing precision on Moderate sea

We first compare MPC-FAA with MPC-NE in scenarios close to *Moderate sea* conditions. Touchdown positions accuracy of both methods shown in Figure 12a is fitted to the normal distribution,

which expresses the mean value of the distance from the center of the landing platform (AprilTag) with the standard deviation. The touchdown success rate of MPC-NE method was 95 %, whereas our method MPC-FAA showed 100 % success rate. Moreover, MPC-FAA method achieved a position deviation 3.5 times smaller than MPC-NE method. The comparison of the vertical approach velocity during the touchdown, shown in Figure 12b, displays that the method MPC-FAA, unlike MPC-NE, ensured that the impact velocity was not higher than  $1 \text{ m s}^{-1}$ .

The graph in Figure 12d shows that MPC-FAA and MPC-NE methods were able to demonstrate accuracy in synchronizing the UAV's roll angle with the USV's. Nevertheless, MPC-FAA achieved a better standard deviation  $2.85^\circ$  compared to MPC-NE with  $3.35^\circ$ . MPC-FAA outperformed MPC-NE with a 2 times smaller standard deviation for the pitch angle deviation (see Figure 12e).

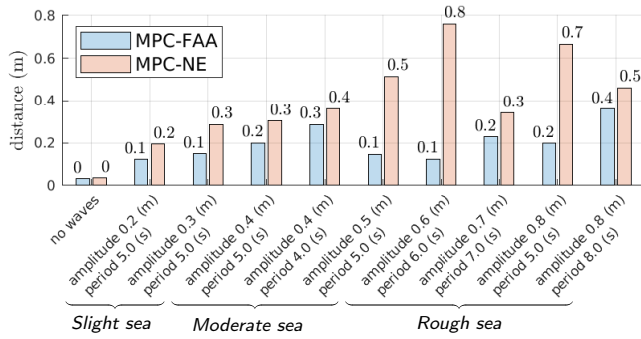
Out of the 95 successful landings achieved by MPC-NE, the landing maneuver was performed within 60 s in all cases (see Figure 12c). However, the average landing time was 34 s, which is 2 times longer than what was achieved by MPC-FAA method. At the same time, as shown in Figure 12a, our approach consistently achieves a higher level of accuracy when landing in *Moderate sea* conditions.

### 5.6.2. Comparison of landing precision in varied sea conditions

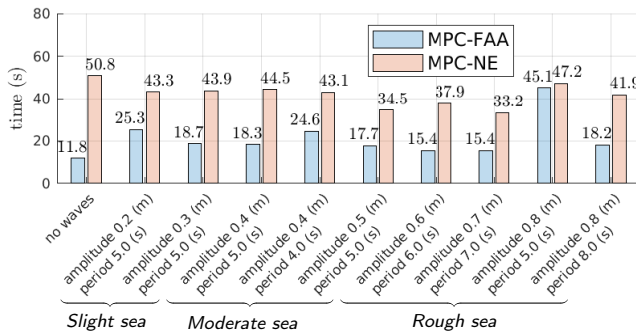
To comprehensively compare MPC-FAA method and MPC-NE method in different conditions, we selected 10 different environment setups that cover a wide range of possible offshore conditions. The simulated scenarios differ in wave amplitude and period, such that the simulated sea varied from *Calm sea* to *Rough sea* (see Table 2). Both MPC-FAA and MPC-NE methods were tested for every scenario one hundred times. The results are shown in (Figure 13 – Figure 14), where the x-axis labels represent the wave amplitude and period used in simulated scenarios, as described in Subsection 5.1.

The comparison of the touchdown position precision is shown in Figure 13a. According to this graph, MPC-FAA achieved a mean touchdown position closer to the center of the USV's deck across all tested scenarios when compared to MPC-NE. Our method's largest average position deviation (37 cm) occurred in a challenging scenario with amplitude 0.8 m and a period of 8 s, where the waves

Model predictive control-based trajectory generation for agile landing of unmanned aerial vehicle on a moving boat

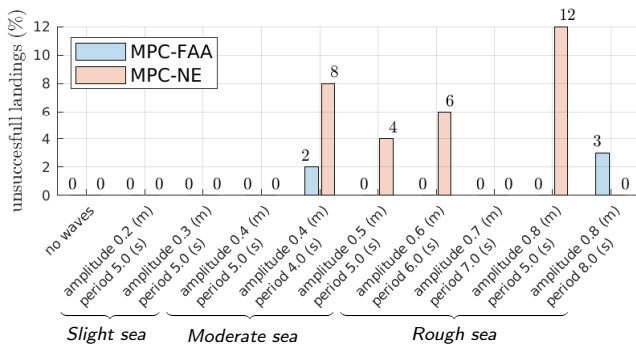


(a) Landing precision as a distance from landing pad center.

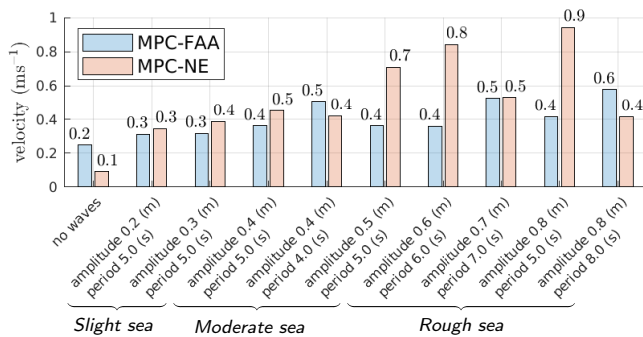


(b) Landing maneuver duration.

**Figure 13:** Comparison of landing maneuver precision and landing duration of the proposed MPC-FAA method and state-of-the-art MPC-NE approach across individual scenario setups.



(a) Number of unsuccessful landings from 100 runs.



(b) Touchdown velocity during the landing.

**Figure 14:** Comparison of the number of unsuccessful landings and touchdown velocity during the landing across individual scenario setups of the proposed method MPC-FAA and state-of-the-art MPC-NE approach.

reached 5 m in height. On the other hand, MPC-NE has the worst touchdown precision when the wave’s amplitude was set to 0.6 m and the period to 6 s. The worst position deviation of MPC-NE is most probably due to the fact that the method neglects the sway and surge movements while the waves affect the USV’s motion in both vertical and horizontal directions.

Figure 13b compares the average duration of the landing maneuvers. Thanks to MPC-FAA method’s ability to use estimation of the USV’s movements before the UAV reached its position, it was ensured that the landing was, on average, 2 times faster than MPC-NE method. The method MPC-NE needs longer observation of the USV’s movements for the purpose of identifying the waves. Moreover, due to neglecting surge and sway movements, UAV may lose sight of the AprilTag, which leads to a termination of the landing maneuver. Based on the data presented in Figure 13b, most landing interruptions of our method occurred in a scenario where the amplitude of the waves was 0.8 m and the period was 5 s. In such a scenario, our method had an average landing duration of around 45 s. However, there was no significant increase in the landing time for the method MPC-NE.

Both methods achieved a low unsuccessful rate of touchdowns, as can be seen in Figure 14a. MPC-FAA method failed only 5 times, while MPC-NE method failed 30 times. The comparison of the vertical approach velocity (see Figure 14b) shows that MPC-FAA method is consistent over all tested scenarios. On the other hand, MPC-NE method ensured a softer landing in scenarios without waves but a more aggressive and dangerous landing in high-wave scenarios. Overall, the proposed method MPC-FAA outperformed MPC-NE in almost every aspect compared and showed that the MPC-FAA is reliable in various sea conditions up to *Rough sea* (wave height 4 m).

## 6. REAL-WORLD EXPERIMENTS

The real-world experiments were conducted in freshwater reservoirs, so to induce conditions similar to those tested in the simulation, it was necessary to create artificial waves. This ensures the repeatability of the experiments over a long time horizon, regardless of the weather, which is responsible for creating the waves on the open waters. The lightweight inflatable mockup of the USV with a landing deck was used for easy manipulation, allowing for the creation of artificial waves with different amplitudes and frequencies.

### 6.1. UAV and USV platforms

The UAV was built using the Tarot T650 frame with Brushless Direct Current Tarot 4114 320KV motors and Turnigy Multistar 51A Electronic Speed Controllers. The UAV was equipped with a Pixhawk 4 autopilot with Global Positioning System (GPS), and powered by a LiPo 6S 8000 mAh battery. The proposed method runs onboard, together with the rest of the autonomy stack, on NUC8i7BEH high-level computer with an i7 8559U processor, 16GB of DDR4 RAM, and a 500GB SSD. The details of the UAV platform are in Hert, , Baca, Petracek, Kratky, Spurny, Petrlik, Vrba, Zaitlik, Stoudek, Walter et al. (2022), however, some modifications were needed due to the UAV’s above-water operation. The UAV was equipped with the RealSense D435 camera for detection of the AprilTag. Furthermore, the myBlueFOX MLC200wG camera was used to observe the UltraViolet (UV) Light-Emitting Diodes (LEDs) that are placed on the USV’s deck. The UAV was equipped with floats on its legs, which ensures the UAV can float in case it lands on the water surface. All electronic components

## Model predictive control-based trajectory generation for agile landing of unmanned aerial vehicle on a moving boat

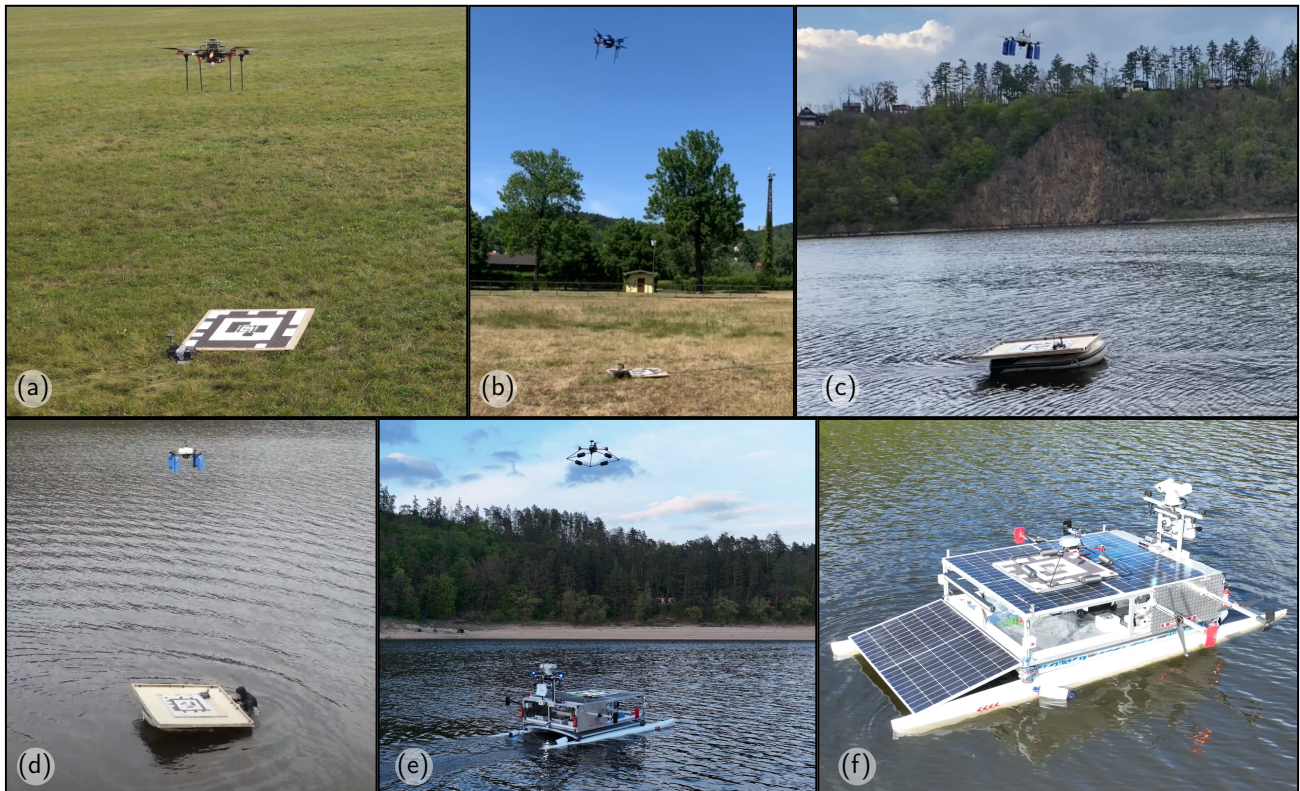


**Figure 15:** Captured photographs from real-world experiments showcasing the method from an initial approach until a precise touchdown. The photos show (a) landing the UAV on the landing pad on land, (b) tracking a moving landing pad with the UAV on land, (c) tracking the USV with the UAV in high wind, (d) tracking the USV with the UAV in high wind and artificial waves, (e) tracking moving USV with the UAV, and (f) UAV successfully landed on the USV. <https://youtu.be/7Cvdttz9Zzk>

were also protected with a water-resistant spray and placed in the 3D-printed water-proofed cover.

For conducting the first experiments, the landing pad was mounted on an inflatable raft towed behind a manned vessel. This mockup, towed by the manned vessel, was later exchanged for the unmanned USV (see Figure 15f). The landing platform was designed in the shape of a square with a side length of 2 m. The Boat unit, which contains a NUC8i7BEH computer, LiPo battery pack, GPS, IMU units, and other electronics, was mounted on the top of a deck. The landing area with a side length of 80 cm was covered with AprilTags and equipped with UV LEDs blinking marker used for relative localization of the USV from the UAV onboard using AprilTag and UVDAR detectors.

It is also worth mentioning that even after a successful touchdown, the UAV can be flipped or dropped from the USV's deck due to the continuous movements of the USV in the waves. To ensure that the UAV remains stable on the deck, the magnetic adhesion device presented in Zhang et al. (2024) can be used to hold the UAV after touchdown. Alternatively, a suitable solution based on docking station Grlj, Krznar and Pranjić (2022) can be used.

## 6.2. Real-world landing on USV

The results from one of the complex real-world experiments are shown in Figure 16, where the comparison of the UAV's and USV's paths in a 2D plane is shown in Figure 16a. The initial segment of the USV's trajectory begins in shallow water near the shore, where we artificially created erratic movements to verify the robustness and precision of the tracking part of MPC-FAA method. The USV is followed by the UAV at the tracking height, where the mutual position is shown in Figure 16b and velocity in Figure 16c.

The velocity was not constant to emulate the USV's movements in a wave environment, allowing us to validate the capability of our method to track the USV even under varying speeds.

The transition to the LANDING phase was intentionally delayed to demonstrate the method's capability to track reliably USV even while turning, thus the landing started at 324 s from takeoff. In the LANDING phase, especially during the touchdown itself, aligning the attitude angles is crucial. Therefore, Figure 16d illustrate the differences between UAV's and USV's attitude angles focused on Descent and Flare states, where our system performs roll and pitch alignment. In contrast, the heading alignment is carried out from the FOLLOW phase, as shown in Figure 16e. The touchdown was executed with a position deviation of approximately 20 cm and an attitude deviation smaller than  $2^\circ$  in every axis.

The next experiment summarized in Figure 17 differs from the previous one by the presence of wind with speed of  $7 \text{ km h}^{-1}$ , wind gusts up to  $17 \text{ km h}^{-1}$  but mainly due to the artificial waves. The comparison of the UAV's and USV's positions over time is shown in Figure 17a. In this experiment, the pilot controlled the first 30 s of the flight to simulate real-world deployment, where the drone is initially controlled by a different program, such as in the motivation scenario, where an exploration planner is used to search for garbage. Afterward, the landing algorithm is started to land from the current location. The UAV was guided from its initial position to the above-water surface. In the first 5 seconds after initiating MPC-based trajectory generator, the UAV gained an altitude  $h_a = 15 \text{ m}$  and began an approach to the USV's position. When the UAV obtained data from the AprilTag detection system, the estimation of the USV's z position was corrected. This phenomenon, which occurred between 55 and 60 seconds from the

Model predictive control-based trajectory generation for agile landing of unmanned aerial vehicle on a moving boat

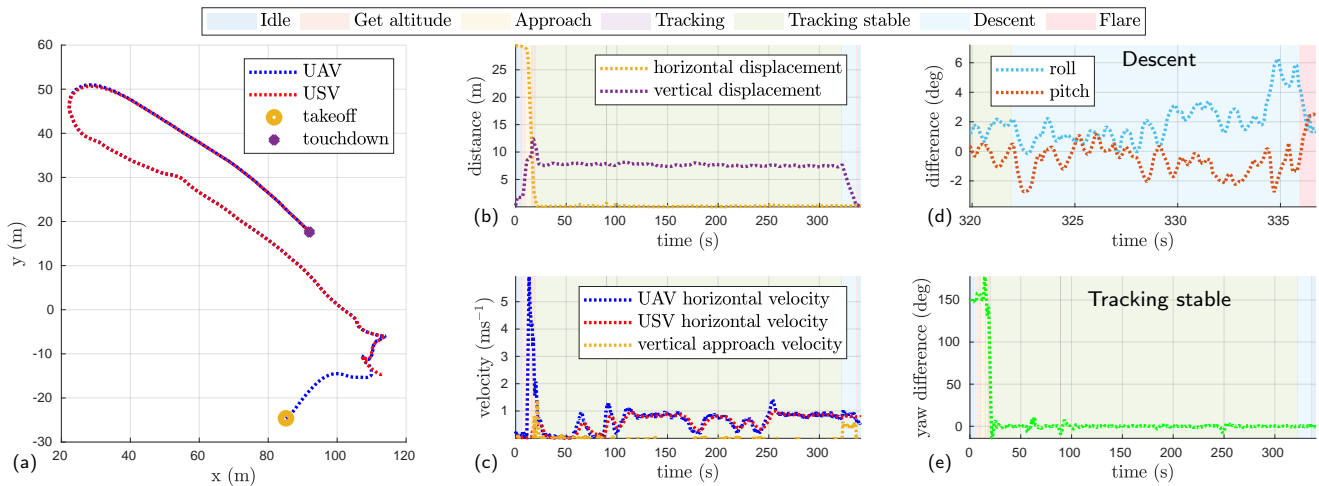


**Figure 16:** Evaluation of the USV following and landing on its deck. Individual graphs depict (a) UAV's and USV's path with marked takeoff and touchdown positions, (b) position displacements between UAV and USV, (c) horizontal velocity together with vertical approach velocity, (d) the difference between the roll and pitch of the UAV and USV during Descent and Flare states, and (e) yaw difference between UAV and USV.

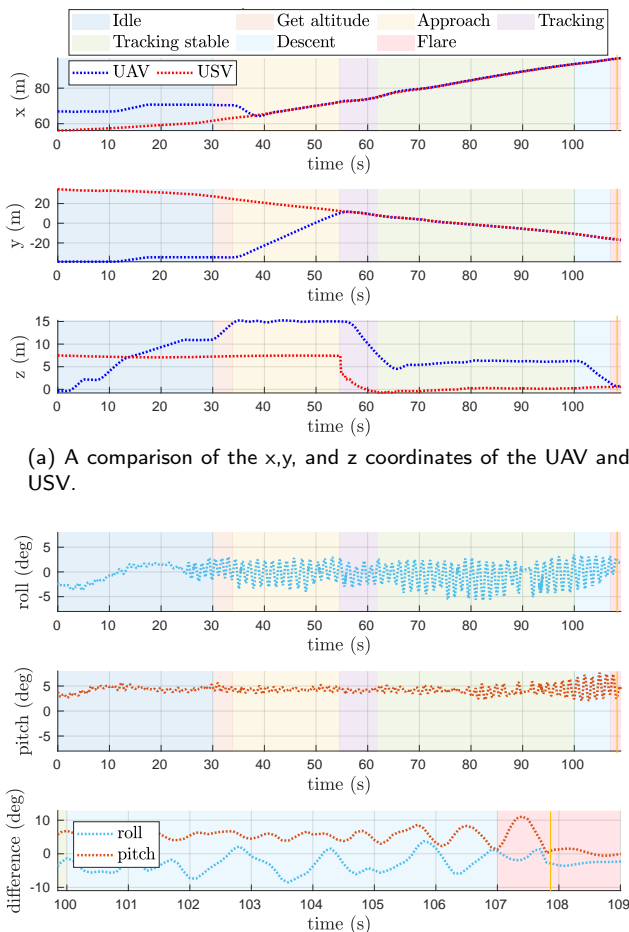


**Figure 17:** Evaluation of the real-world landing experiment with artificial waves. The vertical yellow line indicates a touchdown. <https://youtu.be/U29zBVz3sI>

start, clearly indicates that relying solely on GPS data for estimating the USV's altitude is insufficient and that the estimated altitude can not be used for a safe landing. The conditions for the final landing were met shortly after the tracking of the USV started.

Throughout the entire experiment, the USV was artificially rocked, resulting in a maximum pitch angle of 8° and minimum roll angle of -6° (see Figure 17b). The LANDING phase lasted approximately 8 s and was concluded with a successful touchdown with attitude angles deviation lower than 2° and position deviation approximately 15 cm. The effectiveness of FAA in the reduction of the difference between roll and pitch angles during the flare maneuver is shown in Figure 17c. Despite the significant deviation at the beginning of the Flare state, the increasing penalization of the UAV's attitude effectively reduces this deviation to a minimum until the time of touchdown. During these experiments, we verified that the proposed method can operate in a real-world environment with almost identical behavior to that of simulations.

### 7. Conclusions

In this paper, we proposed a novel method for autonomous trajectory generation of UAV landing on top of a moving and rocking USV. The novel MPC-based trajectory generation relies on the accurate estimation and prediction of USV states, along with precise autonomous control of a UAV. Thanks to the dynamic modification of the penalization matrices, the vertical approach speed is reduced, and attitude angles are aligned with the USV to decrease the impact of the UAV's gear just before the touchdown. The UAV can successfully land in *Moderate sea* conditions or even on *Rough sea* conditions when using our approach. MPC-FAA achieved a reliability rate of 99.5% in harsh conditions in simulated cases, whereas the state-of-the-art approach had 6 times more unsuccessful touchdowns. Moreover, the results of the proposed system indicate a substantial improvement in touchdown accuracy, achieving approximately twice better precision while also completing the landing maneuver 50% faster than MPC-NE method. These outcomes highlight the efficiency of our approach in comparison to existing techniques. Moreover, the MPC-based trajectory generator for landing the UAV on the USV was verified by conducting numerous real-world experiments.



## Model predictive control-based trajectory generation for agile landing of unmanned aerial vehicle on a moving boat

## References

- Abujoub, S., 2019. Development of a landing period indicator and the use of signal prediction to improve landing methodologies of autonomous unmanned aerial vehicles on maritime vessels. Ph.D. thesis. Carleton University.
- Abujoub, S., McPhee, J., Irani, R.A., 2020. Methodologies for landing autonomous aerial vehicles on maritime vessels. *Aerospace Science and Technology* 106, 106169.
- Abujoub, S., McPhee, J., Westin, C., Irani, R.A., 2018. Unmanned Aerial Vehicle Landing on Maritime Vessels using Signal Prediction of the Ship Motion, in: *OCEANS 2018 MTS/IEEE Charleston*, pp. 1–9.
- Akib, A., Tasnim, F., Biswas, D., Hashem, M.B., Rahman, K., Bhattacharjee, A., Fatah, S.A., 2019. Unmanned Floating Waste Collecting Robot, in: *TENCON 2019 - 2019 IEEE Region 10 Conference (TENCON)*, pp. 2645–2650.
- Baca, T., Hert, D., Loiano, G., Saska, M., Kumar, V., 2018. Model Predictive Trajectory Tracking and Collision Avoidance for Reliable Outdoor Deployment of Unmanned Aerial Vehicles, in: *2018 IEEE/RSJ IROS*, pp. 6753–6760.
- Baca, T., Petrlik, M., Vrba, M., Spurny, V., Penicka, R., Hert, D., Saska, M., 2021. The MRS UAV System: Pushing the Frontiers of Reproducible Research, Real-world Deployment, and Education with Autonomous Unmanned Aerial Vehicles. *Journal of Intelligent & Robotic Systems* 102, 1–28.
- Bingham, B., Agüero, C., McCarrin, M., Klamo, J., Malia, J., Allen, K., Lum, T., Rawson, M., Waqar, R., 2019. Toward maritime robotic simulation in gazebo, in: *OCEANS 2019 MTS/IEEE SEATTLE, IEEE*, pp. 1–10.
- Bishop, R.E.D., Price, W.G., 1974. On modal analysis of ship strength. *Proceedings of the Royal Society of London. A. Mathematical and Physical Sciences* 341, 121–134.
- da Cunha, A.E.C., 2015. Benchmark: Quadrotor Attitude Control., in: *ARCH@ CPSWeek*, pp. 57–72.
- DailyPicksandFlicks, 2016. Drone crashes into boat and falls into water. URL: [https://www.youtube.com/watch?v=sQVoPzJ0cZw&t=60s&ab\\_channel=DailyPicksandFlicks](https://www.youtube.com/watch?v=sQVoPzJ0cZw&t=60s&ab_channel=DailyPicksandFlicks). accessed in January 2024.
- Ding, W., Huang, H., 2023. Research on dynamic landing guidance algorithm for the maritime quadrotor. *Ocean Engineering* 271, 113775.
- Doherty, P., Rudol, P., 2007. A UAV Search and Rescue Scenario with Human Body Detection and Geolocalization, in: *Orgun, M.A., Thornton, J. (Eds.), AI 2007: Advances in Artificial Intelligence*, Springer Berlin Heidelberg, Berlin, Heidelberg, pp. 1–13.
- Fortuna, J., Ferreira, F., Gomes, R., Ferreira, S., Sousa, J., 2013. Using low cost open source uavs for marine wild life monitoring-field report. *IFAC Proceedings Volumes* 46, 291–295.
- Fossen, T.I., 2002. Marine control systems—guidance, navigation, and control of ships, rigs and underwater vehicles. *Marine Cybernetics*, Trondheim, Norway, Org. Number NO 985 195 005 MVA, [www.marinecybernetics.com](http://www.marinecybernetics.com), ISBN: 82 92356 00 2.
- Fossen, T.I., 2011. *Handbook of marine craft hydrodynamics and motion control*. John Wiley & Sons.
- García, C.E., Prett, D.M., Morari, M., 1989. Model predictive control: Theory and practice—A survey. *Automatica* 25, 335–348.
- Grlj, C.G., Krznar, N., Pranjic, M., 2022. A decade of uav docking stations: A brief overview of mobile and fixed landing platforms. *Drones* 6.
- Gupta, P.M., Pairet, E., Nascimento, T., Saska, M., 2022. Landing a uav in harsh winds and turbulent open waters. *IEEE Robotics and Automation Letters* 8, 744–751.
- Hert, D., Baca, T., Petracek, P., Kratky, V., Spurny, V., Petrlik, M., Vrba, M., Zaitlik, D., Stoudek, P., Walter, V., et al., 2022. MRS Modular UAV Hardware Platforms for Supporting Research in Real-World Outdoor and Indoor Environments, in: *2022 IEEE ICUAS*, pp. 1264–1273.
- Hert, D., Baca, T., Petrcek, P., Kratky, V., Penicka, R., Spurny, V., Petrlik, M., Vrba, M., Zaitlik, D., Stoudek, P., et al., 2023. Mrs drone: A modular platform for real-world deployment of aerial multi-robot systems. *Journal of Intelligent & Robotic Systems* 108, 64.
- Jalón, M., 2014. Non-linear Attitude Control and Guidance of a Quadrotor UAV. Master's thesis. Lisboa, Técnico.
- Junaid, A.B., Konoiko, A., Zweiri, Y., Sahinkaya, M.N., Seneviratne, L., 2017. Autonomous wireless self-charging for multi-rotor unmanned aerial vehicles. *Energies* 10.
- Kalman, R.E., 1960. A new approach to linear filtering and prediction problems. *Journal of Basic Engineering* 82, 35–45.
- Keller, A., Ben-Moshe, B., 2022. A Robust and Accurate Landing Methodology for Drones on Moving Targets. *Drones* 6.
- Li, N., Huang, H., Wang, X., Yuan, B., Liu, Y., Xu, S., 2022. Detection of floating garbage on water surface based on pc-net. *Sustainability* 14.
- Meng, Y., Wang, W., Han, H., Ban, J., 2019. A visual/inertial integrated landing guidance method for uav landing on the ship. *Aerospace Science and Technology* 85, 474–480.
- Ngo, T.D., Sultan, C., 2014. Nonlinear helicopter and ship models for predictive control of ship landing operations, in: *AIAA Guidance, Navigation, and Control Conference*, p. 1298.
- Novak, F., Baca, T., Prochazka, O., Saska, M., 2024. State estimation of marine vessels affected by waves by unmanned aerial vehicles. URL: [https://mrs.fe1.cvut.cz/data/papers/2024\\_Novak.pdf](https://mrs.fe1.cvut.cz/data/papers/2024_Novak.pdf). Accessed in June 2024.
- Novák, F., Báča, T., Saska, M., 2024. Collaborative object manipulation on the water surface by a uav-usv team using tethers. *arXiv preprint arXiv:2407.08580*.
- Olson, E., 2011. AprilTag: A robust and flexible visual fiducial system, in: *Proceedings of the IEEE International Conference on Robotics and Automation (ICRA)*, IEEE, pp. 3400–3407.
- Paris, A., Lopez, B.T., How, J.P., 2020. Dynamic landing of an autonomous quadrotor on a moving platform in turbulent wind conditions, in: *2020 IEEE International Conference on Robotics and Automation (ICRA)*, IEEE, pp. 9577–9583.
- Persson, L., Wahlberg, B., 2019. Model predictive control for autonomous ship landing in a search and rescue scenario, in: *AIAA Scitech 2019 Forum*, p. 1169.
- Polvara, R., Sharma, S., Wan, J., Manning, A., Sutton, R., 2018. Vision-Based Autonomous Landing of a Quadrotor on the Perturbed Deck of an Unmanned Surface Vehicle. *Drones* 2.
- Raffo, G.V., Ortega, M.G., Rubio, F.R., 2010. An integral predictive/non-linear  $H_\infty$  control structure for a quadrotor helicopter. *Automatica* 46, 29–39.
- Rawlings, J., 2000. Tutorial overview of model predictive control. *IEEE Control Systems Magazine* 20, 38–52.
- Reis, J., Batista, P., Oliveira, P., Silvestre, C., 2023. Discrete-time kalman filter for heave motion estimation. *Ocean Engineering* 277, 114240.
- Sharma, N., Saqib, M., Scully-Power, P., Blumenstein, M., 2022. Sharkspotter: Shark detection with drones for human safety and environmental protection. *Humanity Driven AI: Productivity, Well-being, Sustainability and Partnership*, 223–237.
- Stephenson, J., Duncan, N.T., Greeff, M., 2024. Distributed model predictive control for cooperative multirotor landing on uncrewed surface vessel in waves. *arXiv preprint arXiv:2402.10399*.
- Stingl, A.L., 1970. Vtol aircraft flight system. US Patent 3,487,553.
- Tessendorf, J., 2001. Simulating ocean water. *Simulating nature: realistic and interactive techniques*. SIGGRAPH 1, 5.
- Tian, E., Li, Y., Liao, Y., Cao, J., 2024. UAV-USV docking control system based on motion compensation deck and attitude prediction. *Ocean Engineering* 307, 118223.
- Toffoli, A., Babanin, A., Onorato, M., Waseda, T., 2010. Maximum steepness of oceanic waves: Field and laboratory experiments. *Geophysical Research Letters* 37.
- Venugopalan, T.K., Taher, T., Barbastathis, G., 2012. Autonomous landing of an unmanned aerial vehicle on an autonomous marine vehicle, in: *2012 Oceans*, pp. 1–9.
- Walter, V., Saska, M., Franchi, A., 2018. Fast mutual relative localization of uavs using ultraviolet led markers, in: *2018 International Conference on Unmanned Aircraft Systems (ICUAS)*, IEEE, pp. 1217–1226.
- Wang, J., Olson, E., 2016. Apriltag 2: Efficient and robust fiducial detection, in: *2016 IEEE/RSJ International Conference on Intelligent Robots and Systems (IROS)*, IEEE, pp. 4193–4198.

Model predictive control-based trajectory generation for agile landing of unmanned aerial vehicle on a moving boat

- Xu, R., Liu, C., Cao, Z., Wang, Y., Qian, H., 2024. A manipulator-assisted multiple uav landing system for usv subject to disturbance. *Ocean Engineering* 299, 117306.
- Xu, Z.C., Hu, B.B., Liu, B., Wang, X., Zhang, H.T., 2020. Vision-based Autonomous Landing of Unmanned Aerial Vehicle on a Motional Unmanned Surface Vessel, in: 2020 39th Chinese Control Conference (CCC), pp. 6845–6850.
- Yang, L., Liu, Z., Wang, X., Wang, G., Hu, X., Xi, Y., 2021. Autonomous Landing of a Rotor Unmanned Aerial Vehicle on a Boat Using Image-Based Visual Servoing, in: 2021 IEEE International Conference on Robotics and Biomimetics (ROBIO), pp. 1848–1854.
- Yang, Z., Yu, X., Dedman, S., Rosso, M., Zhu, J., Yang, J., Xia, Y., Tian, Y., Zhang, G., Wang, J., 2022. Uav remote sensing applications in marine monitoring: Knowledge visualization and review. *Science of The Total Environment* 838, 155939.
- Zhang, Y., Wu, Z., Wei, T., 2024. Precise landing on moving platform for quadrotor uav via extended disturbance observer. *IEEE Transactions on Intelligent Vehicles* , 1–10.